The RNA-Binding Protein DND1 Acts Sequentially as a Negative Regulator of Pluripotency and a Positive Regulator of Epigenetic Modifiers Required for Germ Cell Reprogramming

Victor A. Ruthig[1], Matthew B. Friedersdorf[2], Jason A. Garness[1], Steve C. Munger[3], Corey Bunce[1], Jack D. Keene[2], and Blanche Capel[1]

1 Department of Cell Biology, Duke University Medical Center, Durham, NC 27710
2 Department of Molecular Genetics and Microbiology, Duke University Medical Center, Durham, NC 27710
3 The Jackson Laboratory, Bar Harbor, ME, 04609

Abstract

The adult spermatogonial stem cell population arises from pluripotent primordial germ cells (PGCs) that enter the fetal testis around embryonic day 10.5 (E10.5). These cells undergo rapid mitotic proliferation, then enter a prolonged period of cell cycle arrest (G1/G0) during which they transition to pro-spermatogonia. In mice homozygous for the *Ter* mutation in the RNA-binding protein *Dnd1* (*Dnd1*$^{Ter/Ter}$), many germ cells fail to enter G1/G0, and give rise to teratomas, tumors in which many embryonic cell types are represented. To investigate the origin of these tumors, we sequenced the transcriptome of male germ cells in *Dnd1*$^{Ter/Ter}$ mutants at E12.5, E13.5, and E14.5, just prior to the formation of teratomas, and correlated this information with direct targets of DND1 identified by DO-RIP-Seq. Consistent with previous results, we found that DND1 controls the down regulation of many genes associated with pluripotency and active cell cycle, including elements of the mTor, Hippo and Bmp/Nodal signaling pathways. However, DND1 targets also include genes associated with male differentiation including a large group of chromatin regulators activated in wild type but not mutant germ cells during the transition between E13.5 and E14.5. These results suggest multiple functions of DND1, and link DND1 to the initiation of epigenetic modifications in male germ cells.

Introduction

Primordial germ cells (PGCs) are specified at the base of the allantois in mouse embryos at embryonic day (E)6.75, proliferate, migrate through the gut mesentery, and arrive in the gonad between E10.0-E11.0, expressing stem cell markers including SOX2 (SRY-box 2), NANOG (Nanog homeobox), and OCT4 (also known as POU5F1, POU domain, class 5, transcription factor 1) (Matsui et al. (1992); (McLaren, 1995); (Yeom et al., 1996); (Pesce and Scholer, 2000; Yamaguchi et al., 2005). Prior to E12.5, germ line stem cells (EGCs) can be derived readily from the germ cell population (Matsui et al., 1992), and teratomas, a tumor in which all embryonic cell types are represented, spontaneously arise from germ cells in males with a frequency of 1-10% in some strains (Stevens and Little, 1954); (Bustamante-Marin et al., 2013); (Dawson et al., 2018). However, between E12.5 and E15.5, the efficiency of both EGC derivation and teratoma induction declines, presumably reflecting changes that lead to suppression of the underlying pluripotent state of germ cells. These changes are coincident with the entry of male germ cells into G1/G0 cell cycle arrest and their fate transition to pro-spermatogonia (Fig. 1A) (Stevens, 1966); (Western et al., 2011; Western et al., 2010).

A mutation, called *Ter*, that arose spontaneously during routine breeding of 129/SvJ mice, caused a severe reduction in germ cell numbers soon after their specification, and acted as a strong modifier that increased the incidence of spontaneous testicular teratomas to >90% in 129/SvJ mutants (Fig. 1A)(Stevens, 1973). In 2005, *Ter* was mapped to a point mutation that introduced a premature stop codon in the RNA-binding protein (RBP) Dead End 1 *Dnd1* (*Dnd1*^{Ter}) (Fig. 1B) (Youngren et al., 2005). Understanding how DND1 is involved in stabilization of germ cell fate will provide important insights into how this critical process is effected in germ cells and, by analogy, in other stem cell populations from which tumors arise.

The function of DND1 has been studied by knockouts in zebrafish (Gross-Thebing et al., 2017; Weidinger et al., 2003) and mouse (Zechel et al., 2013), and by a conditional deletion at E13.5 in mouse (Suzuki et al., 2016), but none of these mutants formed teratomas, indicating that there is something unique about the *Dnd1*^{Ter} mutation and its

52 129/SvJ genetic background. We have focused our efforts on characterizing the
53 transcriptome in germ cells from *Dnd1*$^{Tet/Ter}$ 129SvT2/SvEMSJ (129T2) mutant embryos
54 just prior to the time when teratomas form (Cook et al., 2009; Cook et al., 2011; Heaney
55 et al., 2012), and cross-referencing this information with direct binding targets of DND1.
56
57 Previous studies have implicated DND1 in both positive and negative regulatory roles.
58 The molecular role of DND1 was first investigated in a human tumor cell line where the
59 protein was shown to bind to the mRNAs of *Cdkn1b* (a negative regulator of the cell cycle)
60 and *Lats2* (a tumor suppressor and negative regulator of p53) to protect these transcripts
61 from miRNA-mediated translational repression (Kedde et al., 2007) perhaps through
62 interaction with APOBEC3 (apolipoprotein B mRNA editing enzyme, catalytic
63 polypeptide-like) (Bhattacharya et al., 2008). Other studies identified targets protected
64 by DND1 in NIH3T3 or HEK293 cells, including the negative cell cycle regulator *Cdkn1b*
65 (cyclin dependent kinase inhibitor 1B)(Cook et al., 2011) and *Ezh2* (enhancer of zeste
66 homolog 2), a mediator of H3K27me3 repression (Gu et al., 2018). Subsequently, two labs
67 showed that DND1 acts as a negative regulator of mRNAs by recruiting targets to the
68 CCR4-NOT deadenylase complex for degradation (Suzuki et al., 2016); (Yamaji et al.,
69 2017). Suzuki et al. showed that DND1 acts as an essential partner of NANOS2 (C2HC-
70 type zinc finger 2, another male-specific RBP) to form P-bodies, and to select and recruit
71 mRNA for degradation. In these studies, conditional deletion of *Dnd1* at E13.5 led to up-
72 regulation of proliferation, meiosis markers, and Caspase3, and the down regulation of
73 several NANOS2 targets associated with male differentiation, similar to *Nanos2* mutants
74 (Suzuki et al., 2016).
75
76 Early studies relied on a candidate approach to identify targets of DND1, which included
77 pluripotency factors and cell cycle genes (Cook et al., 2011; Kedde et al., 2007; Zhu et al.,
78 2011). More recently, Yamaji and co-workers performed photoactivatable-Ribonuleoside-
79 Enhanced Cross-Linking and Immunoprecipitation (PAR-CLIP) assays in HEK293 cells,
80 and investigated the expression of identified targets in induced primordial germ like cells
81 (PGLCS) and germ line stem cells derived from adult spermatogonia. Consistent with
82 Suzuki's results, Yamaji et al. showed that DND1 acts with CCR4-NOT to destabilize and
83 repress RNAs associated with apoptosis, inflammation and signaling pathways including

84 TgfB, Wnt, and PI3K-AKT. Extrapolating results from these in vitro cell types, Yamaji et
85 al. suggested that activation of pluripotency genes, as well as TgfB and inflammatory
86 signaling genes, contribute to the formation of teratomas in gonadal germ cells (Yamaji
87 et al., 2017).
88
89 We sequenced the transcriptome of male germ cells in *Dnd1*$^{Ter/Ter}$ mutants at E12.5, E13.5,
90 and E14.5, just prior to the formation of teratomas, and correlated this information with
91 direct targets of DND1. We identified direct transcript targets of DND1 using an
92 independent method, Digestion Optimized-RIP-seq (DO-RIP-seq), after expressing a
93 tagged DND1 protein in HEK293 cells. We cross-referenced our DO-RIP-seq targets with
94 the PAR-CLIP results from Yamaji et al., and compared the transcript levels of nontargets
95 and targets common to both RNA-immunoprecipitation assays in isolated germ cells from
96 129T2-*Dnd1*$^{Ter/Ter}$ and *Dnd1*$^{+/+}$ littermates at E12.5, E13.5 and E14.5. Consistent with our
97 previous results and the molecular models proposed by Suzuki and Yamaji, between
98 E12.5-E13.5 DND1 controls the down regulation of many genes associated with
99 pluripotency and cell cycle, including elements of the both the Hippo and Bmp/Nodal
100 signaling pathways. However, we found that DND1 targets include many genes associated
101 with male differentiation including a large group of chromatin regulators normally
102 activated during the second transition between E13.5 and E14.5. These results suggest
103 multiple functions of DND1, and link DND1 to the initiation of epigenetic modifications
104 in male germ cells.
105
106 **Materials and Methods**
107
108 **Mice, timed matings, and genotyping**
109 *Dnd1*$^{Ter/+}$ mice were kindly provided by Dr. Joseph Nadeau and maintained on a
110 129T2/SvEmsJ background. 129T2/SvEmsJ (hereafter referred to as "129T2";
111 https://www.jax.org/strain/002065) was predicted to be the closest living strain at The
112 Jackson Laboratory (JAX) to the original 129/SvJ strain on which *Ter* arose. Because the
113 formation of teratomas is a 129-strain-specific phenotype, to generate mutants in which
114 germ cells were fluorescently tagged, Oct4-EGFP (originally on a mixed genetic
115 background) (Yoshimizu et al., 1999) was back-crossed to 129T2-*Dnd1*$^{Ter/+}$ for 9

116 generations, then crossed to 129T2-*Dnd1*$^{Ter/Ter}$ mutant females to generate 129T2-
117 *Dnd1*$^{Ter/+}$*;Oct4-EGFP* male and female heterozygotes. For timed matings, heterozygotes
118 were intercrossed, females were checked for plugs, and staged as day E0.5 if positive. For
119 genotyping, tail DNA was extracted using standard methods and genotyped using the
120 following primer sets: GFP-F 5- AAG TTC ATC TGC ACC ACC G and GFP-R 5- TCC TTG
121 AAG AAG ATG GTG CG and Ter-F 5-GTA GTT CAG GAA CTC CAC TTG TG-3, Ter-R 5-
122 GCT CAA GTT CAG TAC GCA C-3. *Dnd1*^{Ter} mice were genotyped by PCR using an
123 annealing temperature of 62°C. The PCR product (145 bp) was digested overnight at 37°C
124 with the restriction enzyme *DdeI* and run on a 4% agarose gel or 6% acrylamide gel. *DdeI*
125 digestion of DNA from mice with the *Dnd1*^{Ter} mutation produces 123 bp and 22 bp
126 products.
127
128 **FACS, RNA isolation, Library Preparation**
129 Global gene expression was quantified by RNA sequencing (RNA-seq) in germ cells at
130 multiple embryonic stages. To isolate germ cells, embryos were collected at E12.5, E13.5,
131 and E14.5. The gonad was isolated from XY embryos, and incubated in 250 ml 0.25%
132 Trypsin EDTA (Gibco #25200) at 37ºC for 5–10 minutes. The trypsin was removed and
133 replaced with 400 ml PBS with or without 4 ml RNase-free DNase (Promega #M6101).
134 The tissue was dissociated, and the cells were passed through a 20µm cell strainer (BD
135 Falcon #352235). Fluorescence activated cell sorting (FACS) was performed by the Duke
136 Comprehensive Cancer Center Flow Cytometry Shared Resource. Between 200-900
137 EGFP+ cells were sorted into 100 µl Qiagen Buffer RLT (from RNeasy Micro Kit, Qiagen
138 #74004) +DTT, without carrier RNA and frozen at -80ºC.
139
140 Total RNA was extracted from purified germ cell aliquots and eluted in 13 µl of
141 RNase/DNase free water using the Qiagen RNeasy Micro Kit (Qiagen #74004) with on
142 column DNase digestion following manufacturer's protocols. Next, 10 µl of RNA eluate
143 went directly into first strand synthesis, using oligo-dT primers according to the Smart-
144 seq2 protocol (Picelli et al., 2014) scaled for input. Pre-amplification mix was prepared
145 according to the Smart-seq2 protocol, scaled to 27 µl input from the first strand synthesis
146 reaction. DNA was purified using the recommended Agencourt AMPure XP bead kit
147 (Beckman Coulter #A63880), DNA was quantified by fluorometric quantitation (QUBIT).

148 0.5 ng from each sample was brought forward for tagmentation using the Nextera XT
149 DNA Sample Prep Kit (illumina #15032352). Samples were size-selected using a 0.6 ratio
150 of SPRIselect beads (Beckman Coulter #B23317) to DNA to obtain fragments >300 bp.
151 Samples were eluted from beads according to protocol, and submitted to the Duke
152 Sequencing Facility for QC by QUBIT and by traces run on an Agilent 2100 bioanalyzer
153 to determine library sizes. The concentration of each library was normalized and 8 pmoles
154 of the pool were sequenced using 50bp SR on the Illumina Hi-seq 2500. Eight samples (4
155 mutant and 4 wild type) were pooled for each stage and run in technical replicate in 2
156 lanes of a flow cell. The Duke Sequencing Facility used FastQC for preliminary quality
157 control.
158
159 **Transcriptome processing and mapping reads**
160 There were ~22M reads/sample at E12.5, ~15M reads/sample at 13.5, and ~38M
161 reads/sample at 14.5. Bowtie 2 was used to align the RNA-seq reads to mm9 using default
162 settings. >81% of E12.5 transcripts aligned to the genome, whereas that number for >87%
163 at E13.5, and >92% at E14.5. The Cufflinks pipeline (version 2.2.0) (Top-Hat, Cufflinks,
164 Cuffmerge) was used to assemble transcripts using default settings. We considered only
165 those transcripts previously annotated using Ensembl75. Gene levels were quantified
166 using Cuffquant, and differential expression analysis was performed using Cuffdiff. This
167 data was used for further analyses.
168
169 **Filtering the datasets** We found that some of the most significant outlier genes are
170 strongly expressed in Leydig and Sertoli cells based on the Jameson datasets (Jameson et
171 al., 2012) (Suppl. Fig. 1). Most of these genes were upregulated between E13.5 and E14.5
172 in mutant samples. We considered the possibility that this might reflect partial
173 transdifferentiation of germ cells to express genes associated with somatic lineages, but
174 using fluorescent immunocytochemistry we did not detect any co-localization of markers
175 (data not shown). Because the intensity of *Oct4-EGFP* fluorescence declines, and the
176 number of germ cells in mutants is reduced at E14.5, we suspected that contamination by
177 somatic cell types in the gonad during fluorescence activated cell-sorting (FACS)
178 accounted for this problem. As a means to eliminate any transcripts that might be due to
179 contamination by another cell type, cell-type-specific microarray data from the Jameson

et al. study, for stages E11.5, E12.5 and E13.5, was used to generate lists of all genes enriched in the male germ cell population. Lists from E11.5 and E12.5 in the Jameson array were applied to the E12.5 and E13.5 transcriptome data sets. The list from E13.5 in the Jameson array was applied to the E13.5 and E14.5 transcriptome data sets. Only genes appearing on these lists were retained in the filtered RNA-seq data (1213 genes for E12.5-E13.5, and 1207 genes for E13.5-E14.5). The filtered datasets were replotted and used for this analysis. A similar method was used to generate lists of genes specifically enriched and depleted in all germ cells, female germ cells and male germ cells at E12.5 and E13.5 (E12.5 or E13.5 lists from Jameson Array applied to E12.5 or E13.5 transcriptome data sets respectively) . These lists were used for heat map analysis.

RepEnrich Analysis To evaluate the status of repetitive elements (specifically transposable elements), the original unfiltered raw data for wild type and *Dnd1*$^{Ter/Ter}$ samples were compared using RepEnrich (Criscione et al., 2014). The protocol for library preparation, mapping and differential enrichment analysis (Robinson et al., 2010) was followed as described by (Greco et al., 2016) and detailed by SW Criscione (https://github.com/nskvir/RepEnrich) with minor adjustments. Briefly, Bowtie 1.2.1 was used (Langmead et al., 2009) and the custom repetitive annotation was prepared using parameters: -p 6 -q -m 1 -S --max. For statistical analysis, a FDR (false discovery rate) of less than 0.05 was used as the cutoff for significance (Greco et al., 2016); (Criscione et al., 2014).

Gene Set Enrichment Analysis and Ingenuity Pathway Analysis

Gene set enrichment analysis was performed using GSEA v3.0, build 0160 (http://software.broadinstitute.org/gsea/) as described in (Subramanian et al., 2005). "Log2 ratio of classes" was used to rank changes in gene expression between developmental stages as well as between wild type and *Dnd1*$^{Ter/Ter}$ samples. Normalized Enrichment Scores (NES) and FDR values were used to describe the magnitude of change and the significant enrichment of the gene sets respectively.

Ingenuity Pathway Analysis. Differentially expressed genes (DEGs) were assessed for statistical enrichment/depletion of specific pathways using the Qiagen Ingenuity Pathway

212 Analysis (IPA) database (Application build: 470319M; Content version: 43605602).
213 DEGs included those that were differentially expressed 1) between developmental stages
214 within a *Ter* genotype class, and 2) between *Ter* genotype classes at a specific stage. The
215 cutoff for inclusion in the IPA analysis was set at a differential expression FDR < 0.01.
216
217 **Dnd1 DO-RIP-seq.** DO-RIP-seq was performed as described in (Nicholson et al., 2017).
218 Briefly, 5 - 15 cm^2 plates of HEK293 cells were transfected with ~35 µg/plate FLAG-DND1
219 or untagged DND1 (as a negative control), grown for 24hrs, then harvested in PLB.
220 Lysates were treated with 50 U/µg of MNase for 5 min at 30°C, and FLAG
221 immunoprecipitations were performed. RNA from IPs was radiolabeled and run on a 10%
222 TBE-Urea gel. RNA fragments from ~25-75 nucleotides were excised and extracted from
223 the gel. cDNA libraries were prepared using the NEBNext Multiplexing Small RNA
224 Library Prep Set for Illumina with 14-17 rounds of amplification, following the
225 manufacturer's protocol with the exception that the 5' RNA adapter was replaced with a
226 custom 5' adapter compatible with UMI (Unique Molecular Identifier) tagging (Kivioja et
227 al., 2011) (RNA adapter sequence GUUCAGAGUUCUACAGUCCGACGAUCNNNNN). In
228 addition to DND1, negative control IPs input samples were also prepared for sequencing
229 in a similar fashion using 17 rounds of amplification. An aliquot of the MNase-digested
230 lysate prior to IP was set aside for generating input libraries. rRNA depletion was
231 performed on input samples using the Epicenter Ribo-Zero Gold rRNA removal kit. Input
232 RNA was size selected and libraries were prepared as described above for the IP samples.
233 All experiments were performed as biological duplicates.
234
235 Libraries were sequenced using Illumina HiSeq 2500. Processing of data was performed
236 as described in Nicholson et al. After removal of adapter and UMI sequences, reads were
237 mapped to hg19 using TopHat2. Binding sites were identified using the binning and
238 normalization procedure of Nicholson et al. (Nicholson et al., 2017), IPs were compared
239 to input samples to identify sites enriched in DND1 IPs. Reads with a low pass filter of >3
240 reads and >1.5 fold enrichment over input were considered DND1 binding sites.
241
242 **Results**
243

244 ***Dnd1$^{Ter/Ter}$* mutant germ cells are delayed in the germ cell transcriptional**
245 **profile relative to wild type at E12.5.** To investigate the changes in *Dnd1$^{Ter/Ter}$*
246 mutant germ cells relative to wild type, 129T2-*Dnd1$^{Ter/+}$; Oct4-EGFP* males and females
247 were intercrossed, and ~600 germ cells were isolated by FACS from 4 independent
248 homozygous and wild type fetal gonads at each of 3 stages, E12.5, E13.5 and E14.5, after
249 germ cells have populated the gonads, and prior to teratoma detection (Fig. 1A; (Cook et
250 al., 2011)). Sequencing was performed, reads were mapped to the genome, and a reads
251 per kilobase transcript per million (RPKM) value was calculated for each transcript.
252 RPKM values used in our analysis are provided with the capability to generate an
253 expression graph for any gene, as a user-friendly resource for the community (Suppl.
254 Table 1).
255
256 The *Dnd1* transcript was detected at similar levels in wild type and homozygous mutant
257 germ cells at E12.5 (Fig. 1B), but showed a rapid decline at later stages (data not shown).
258 The *Ter* mutation, predicted to lead to a premature stop codon (Youngren et al., 2005) is
259 evident in the third exon of *Dnd1* and efficiently distinguishes wild type and mutant
260 samples (Fig. 1B, blue arrow). The 129T2 variant of a SNP that differs between B6 and 129
261 was detected in the 3'UTR of all samples confirming the 129T2 strain background (red
262 arrow).
263
264 *Dnd1* is expressed in both XX and XY germ cells from early migratory stages (Youngren
265 et al., 2005). In *Dnd$^{Ter/Ter}$* mutants, many germ cells are lost prior to arrival in the gonad
266 (Cook et al., 2009; Noguchi and Noguchi, 1985). Given that loss of RBPs in germ cells of
267 other species results in transdifferentiation to somatic fate (Ciosk et al., 2006; Gross-
268 Thebing et al., 2017; Updike et al., 2014), we investigated the possibility that *Dnd1$^{Ter/Ter}$*
269 mutant germ cells were significantly altered by the time they populated the gonad, and
270 did not retain their germ cell identity. The top two principle components account for 43%
271 and 25% of the observed variation in the top 500 most variable protein-coding genes.
272 Based on the variability captured by Principle Component (PC) 1, it appears that E13.5
273 mutant germ cells cluster more closely with E12.5 wild type germ cells while E12.5 mutant
274 germ cells are delayed. Further, PC2 appears to stem mainly from expression variation in
275 E14.5 *Dnd1$^{Ter/Ter}$* germ cells, suggesting that the transcription profile in these mutant

276 germ cells continues to diverge from a normal trajectory (Fig. 1C). To investigate these
277 differences further, we compared expression in *Dnd1*$^{Ter/Ter}$ mutant germ cells with a list of
278 genes specific to germ cells (Fig. 1D) and a list of genes that distinguish *male* germ cells
279 (Suppl Fig. 2A) at E12.5 and E13.5. These lists include genes that characterize germ cells
280 by their specific expression in this lineage, and those that characterize germ cells by their
281 specific repression (eg. somatic genes)(Jameson et al., 2012). Based on heat map analysis,
282 *Dnd1*$^{Ter/Ter}$ mutant germ cells show an overall pattern similar to wild type male germ cells
283 for both up- and down-regulated genes at E12.5 and E13.5. For example, both *Ddx4* (dead
284 box helicase 4)(*Vasa*) and *Dazl* (deleted in azoospermia like) show a delay in activation,
285 similar levels at E13.5, and a down regulation at E14.5, while *Stella (Dppa3*
286 (developmental pluripotency associated protein 3)*)*, a germ cell specific gene, and *Prdm1*
287 (PR/SET domain 1) (*Blimp1*) show no significant differences from wild type at any stage
288 (Fig. 1E). These data indicate that although *Dnd1*$^{Ter/Ter}$ germ cells have a delayed gonadal
289 differentiation program, they have a transcriptome similar to wild type germ cells soon
290 after they arrive in the gonad.
291
292 **Neither the female germ cell program nor other embryonic pathways are**
293 **activated in XY *Dnd1*$^{Ter/Ter}$ germ cells.** Because *Dnd1* expression becomes specific to
294 the male pathway after germ cells enter the gonad (Youngren et al., 2005), we next
295 investigated whether there was evidence for a shift to the female germ cell-specific
296 program in *Dnd1*$^{Ter/Ter}$ male germ cells by comparing expression in mutants to a list of
297 genes specific to female germ cells (Jameson et al., 2012). A heat map comparison showed
298 little evidence for ectopic activation of female pathway genes (Suppl. Fig. 2B). Based on a
299 cumulative distribution plot, few female-specific genes were significantly altered in
300 mutants at E13.5 (Suppl. Fig. 2C). In contrast to their pattern in wild type female germ
301 cells, genes that are associated with entry into meiosis (eg. *Stra8* (stimulated by retinoic
302 acid 8)*, Sycp3* (synaptonemal complex protein 3)) were not upregulated in *Dnd1*$^{Ter/Ter}$
303 mutant XY germ cells (Suppl. Fig. 2D). However, some genes that become female-specific
304 by downregulation in male germ cells (eg. *Rhox9* (reproductive homeobox 9) and *Rhox6*)
305 showed a less robust downregulation at the stage when male and female germ cell
306 pathways diverge (E12.5) (Suppl. Fig. 2E). In general, these were genes associated with
307 the pluripotent state of early germ cells.

308

309 Many genes associated with developmental pathways carry bivalent marks in germ cells
310 (Lesch and Page, 2014). Because teratoma development is associated with the
311 upregulation of developmental pathways, we investigated whether specific groups of
312 bivalent genes showed upregulation in *Dnd1*$^{Ter/Ter}$ germ cells. We found no evidence of
313 lineage infidelity based on the activation of any subgroup of bivalent genes associated
314 with embryonic pathways (Suppl. Fig. 3A), or significant differences in specific factors
315 associated with differentiation (Suppl. Fig. 3B).

316

317 **Homozygosity for the *Dnd1*^{Ter} mutation is associated with subtle changes in**
318 **expression of many genes in male germ cells between E12.5-E14.5.**

319 Next we compared the effect of the *Ter* mutation on the temporal gene expression of germ
320 cells during the transition between E12.5 and E13.5 and between E13.5 and E14.5. While
321 most expressed genes retain a similar temporal pattern in the mutant compared to wild
322 type over this period, hundreds are up- and down-regulated between E12.5-13.5 and/or
323 E13.5-14.5 (Fig. 2A). More genes are up-regulated in mutant PGCs relative to wildtype
324 during the first transition between E12.5-13.5 (151 up v. 58 down), whereas more genes
325 are down-regulated in mutant PGCs during the second transition between E13.5-14.5 (43
326 up v. 266 down). Transcripts for many pluripotency genes are enriched in mutant PGCs
327 throughout the time course (Fig. 2B). A large group of genes associated with the initiation
328 of male germ cell development, including *Nanos2*, *Nanos3* (C2HC-type zinc finger 3), *Ret*
329 (rearranged during transfection – a receptor tyrosine kinase), *Ddx25* (dead box helicase
330 25), and *Dppa4* (developmental pluripotency-associated protein 4), a marker of
331 pluripotent cells required for differentiation (Madan et al., 2009) fail to be activated in
332 mutants (Fig. 2C). Based on Gene Set Enrichment Analysis (GSEA), targets of DPPA4
333 (including *Gtsf1* (gametocyte specific factor 1), *Stk31* (serine threonine kinase 31), *Ddx4*
334 (dead box helicase 4), *Iqcg* (IQ motif containing G), *Mael* (maelstrom spermatogenic
335 transposon silencer), *Slc25A31* (solute carrier famly 25), *Rnf17* (ring finger protein 17),
336 and *Mep1b* (meprin A subunit beta), Suppl. Table 2) are enriched in wildtype PGCs (Fig.
337 2D, left panel) but not in mutant PGCs (Fig. 2D, right panel) during the E13.5-E14.5
338 transition, further suggesting that the *Ter* mutation disrupts *Dppa4* expression and its

339 downstream function in PGCs.

340

341 Given the critical roles of *Nanos2* in establishing the male pathway in mouse germ cells
342 (Suzuki and Saga, 2008), we asked whether most transcriptional changes in *Dnd1*$^{Ter/Ter}$
343 mutants could be accounted for by failure to activate *Nanos2* (Fig. 2C). To investigate this
344 possibility, we compared the transcriptome changes between the two mutants. Although
345 some genes changed in a similar manner (eg. genes associated with pluripotency), many
346 genes exhibit opposing patterns (Fig. 2E). For example, *Ret* was not affected in *Nanos2*
347 mutants whereas *Sycp3* and *Stra8* were elevated (Saba et al., 2014). In *Nanos2* mutants,
348 *Nan*os3 was upregulated, whereas in *Dnd1* mutants, it was not (Fig. 2C; see Suppl. Table
349 3 and for full data set). This indicates that DND1 is upstream of both Nanos genes, and is
350 consistent with the finding that *Nanos3* can partially rescue the *Nanos2* mutants (Saba et
351 al, 2014).
352

353 **Transposable Elements and piRNA pathways were not strongly affected by**
354 **E14.5, despite the failure to activate their repressors.**

355 Several genes involved in repression of transposable elements including *Piwil4* (piwi like
356 RNA-mediated gene silencing 4), *Tdrd5* (tudor domain containing 5), *Morc1* (MORC
357 family CW-type zinc finger 1), and *Mael* were either not activated or expressed at much
358 lower levels in mutants (Fig. 2F). Proteins encoded by these genes normally silence LINE
359 and other transposable elements. Our transcriptome data was based on oligo-dT priming,
360 however some transposable elements contain polyadenylation sites (Lee et al., 2008). We
361 interrogated the raw transcriptome data at E14.5 for activation of transposable/repetitive
362 elements using RepEnrich, a program optimized to detect differential enrichment
363 between two RNA-seq datasets (Criscione et al., 2014). Very few transposable element
364 reads showed a significant difference between wild type and mutant germ cells (FDR <
365 0.05) (Fig. 2G). This trend of similarity between wild type and mutant germ cells was also
366 observed when we interrogated repetitive elements and transposable elements more
367 generally (Suppl. Fig. 4A,B).
368

369 DND1 was previously reported to protect transcripts from miR470 (in zebrafish) and mir-
370 1, miR-206, and miR-221 (in human cell lines) -mediated degradation (Kedde et al.,
371 2007). Therefore, we predicted that targets of a mouse ortholog of these miRNAs such as
372 miR302 (the ortholog of zebrafish miR470) would be down-regulated in the absence of
373 DND1 protection. However, only *Lats2* (large tumor suppressor kinase 2) showed this
374 behavior; other targets of miR302 were elevated in *Dnd1*$^{Ter/Ter}$ germ cells relative to
375 wildtype (Suppl. Fig. 5A). We used Ingenuity Pathway Analysis (IPA-Qiagen) to infer
376 activation of individual miRNAs on a global basis. IPA compares the behavior of sets of
377 miRNA targets among samples, calculates a p-value based on this overlap, and returns a
378 Z-score reflecting the probability that a particular miRNA pathway is activated or
379 repressed based on the expression of target genes. Based on IPA analysis, only one
380 miRNA (mir223) cleared the activation cut-off of 2 between E13.4 and E14.5 in mutant
381 cells (Suppl. Fig. 5B). However, investigation of the expression of predicted targets of
382 mir223 revealed no consistent pattern (data not shown). Overall, we discovered no strong
383 miRNA regulatory signature in this mRNA-seq analysis.
384
385 **Identification of DND1 direct targets.** We identified hundreds of genes that were
386 up- and down-regulated between E12.5-14.5 in DND1 mutant PGCs (Fig. 2A). DND1 has
387 been shown to both promote degradation of target transcripts (Suzuki et al., 2014; Yamaji
388 et al., 2017) and to stabilize other target transcripts by competing for miRNA binding sites
389 (Kedde et al., 2007; Zhu et al., 2011). We were interested in whether genes in both up-
390 and down-regulated categories were direct targets of DND1.
391
392 *Dnd1* shares sequence similarity with genes encoding five other RNA binding
393 proteins (*Rbm46* (RNA binding motif protein 46), *A1cf* (APOBEC complementation
394 factor), *Rbm47*, *Syncrip* (synaptotagmin binding cytoplasmic RNA interacting protein)
395 and *Hnrnpr* (heterogeneous nuclear ribonucleprotein R). All members of this subfamily
396 contain three RNA recognition motifs (RRMs) except DND1 which contains two RRMs.
397 Additionally, three members of the family, including DND1, contain a C-terminal double
398 stranded RNA binding domain (DSR). (Fig. 3A). The *Ter* mutation generates a
399 premature stop codon in the middle of RRM2 (arrow). To identify binding sites of DND1
400 we performed DO-RIP-seq (Nicholson et al., 2017) in HEK293 cells, using a tagged mouse

401 DND1. The most enriched motif in DND1 binding sites was DAUBAW (D=A, G or U, B=C,
402 G or U and W=A or U), a motif that is very similar to the known RNA motif of RBM47, its
403 closest relative (Fig. 3B). The RBM47 motif defined by RNA-Compete (Ray et al., 2013) is
404 GAUSAW (S=G or C and W=A or U), both the DND1 and RBM47 motifs contain AU in
405 the second and third position and AW in the fifth and sixth, but differ in the first and
406 fourth position where the recognition sequence is more degenerate. Although *Rbm47*
407 expression declines sharply between E12.5 and E14.5, *Rbm46*, *Rbm47*, *Syncrip*, and
408 *Hnrnpr* are all expressed in germ cells in the gonad, and could partially compensate for
409 loss of DND1 (Suppl. Fig. 6).
410
411 Compared to their proportional representation across the whole transcriptome, DND1
412 binding sites were strongly over-represented in 3' untranslated regions (UTRs) and to a
413 lesser extent in the coding sequence (CDS) (Fig. 3C). Targets identified by DO-RIP-seq
414 largely agree with PAR-CLIP identified DND1 targets from Yamji et al, with 2953 mRNAs
415 shared in common (Yamaji et al., 2017)(Fig. 3D). This represents a significant overlap
416 ($p<0.001$) based on 1000 iterations of randomly shuffled binding sites matched for size
417 and restricted to expressed 3'UTRs.
418
419 **Direct targets of DND1 are both up- and down-regulated in *Dnd1*$^{Ter/Ter}$**
420 **mutants.** Because RIP assays were not conducted in germ cells due to the absence of
421 appropriate antibodies or transgenic tags, we first identified the set of conserved targets
422 expressed in germ cells (1347 out of 2953 targets). Next we investigated the relationship
423 between number of DND1 binding sites in the target transcript (1 to 9+ binding sites) and
424 its expression in wild type and 129T2 *Dnd1*$^{Ter/Ter}$ mutant germ cells between E12.5-E13.5
425 and E13.5-E14.5. Cumulative distribution function (CDF) plots were
426 generated comparing RNA abundance changes for transcripts classified by number of
427 DND1 binding sites (non-targets, 1 site, 2 sites, etc). Changes in RNA abundance were
428 evaluated in this manner for four conditions: E12.5-E13.5, and E13.5-E14.5 in both
429 mutant and wild type germ cells. In wild type germ cells, the presence of more DND1
430 binding sites in a target transcript was correlated with a higher likelihood of down-
431 regulation relative to transcripts with few or no target sites during the transition between
432 E12.5-E13.5, while the opposite pattern was observed between E13.5-E14.5 – target

433 transcripts with more DND1 binding sites were more likely to be up-regulated relative to
434 non-targets. During this later transition, DND1 targets tend to change faster than the rest
435 of the transcriptome (Fig. 3E). In 129T2-*Dnd1*$^{Ter/Ter}$ mutants, DND1 targets behave more
436 like non-targets, reflecting the effect of the *Ter* mutation on DND1 function.
437
438 Overall, among targets of DND1, cell cycle genes and chromatin regulators were over-
439 represented (Fig. 4A; Table 4). Overlapping binding sites from all three RIP assays were
440 present in the 3'UTR of the cell cycle gene, *Ccne1*, and throughout the CDS and 3'UTR of
441 the chromatin regulator, *Kat7* (lysine acetyltransferase 7) (Fig. 4B). In addition to *Ccne1*,
442 *Rheb* (Ras homolog enriched in brain) and *Rhob* (Ras homolog family member B), two
443 GTP-binding proteins associated with active cell cycle were targets of DND1, and were
444 elevated in the mutant transcriptome along with *Trp57* (*Cdkn1c*, cyclin dependent kinase
445 inhibitor P57), which was not expressed in HEK293 cells (Fig. 4C). *Kat7* and other
446 chromatin regulators, including *Setdb1* (set domain bifurcated 1), *Kdm5a* (lysine
447 demethylase 5a), and *Rbbp5* (RB Binding Protein 5, Histone Lysine Methyltransferase
448 Complex Subunit) mapped as targets, and all lagged behind wild type levels (Fig. 4D), as
449 did many other chromatin regulators not expressed in HEK293 cells (Suppl. Fig. 7).
450
451 Many genes associated with signaling pathways were identified as targets of DND1, and
452 were significantly changed in mutants (Fig. 5A). A large group of genes associated with
453 the BMP signaling pathway, were elevated in mutant germ cells (Fig. 5B), as also reported
454 by Yamaji (Yamaji et al., 2017). We identified elements of other signaling pathways
455 elevated in mutants that map as targets of DND1, including *Ywhah* (tyrosine 3-
456 monooxygenase/tryptophan 5-monooxygenase activation protein eta), *Ywhag* (tyrosine
457 3-monooxygenase/tryptophan 5-monooxygenase activation protein gamma), *Csnk1e*
458 (casein kinase 1 epsilon), *Yap1* (yes-associated protein 1), and *Prkci* (protein kinase C lota)
459 in the Hippo pathway (Fig. 5C). In contrast, transcripts for two central genes in the mTOR
460 pathway that mapped as direct targets of DND1, *Rictor* (rapamycin-insensitive
461 companion of mTOR) and *Mtor* (mammalian target of rapamycin), were down-regulated
462 in mutants (Fig. 5D).
463

464 **Ingenuity Pathway Analysis identified apoptotic and cell cycle pathways as**
465 **strongly affected in mutants.** We used Ingenuity Pathway Analysis (Qiagen) to
466 identify curated pathways most strongly affected in the mutant transcriptome. This
467 analysis resulted in the identification of Cellular Growth and Proliferation (482 genes)
468 and Cell Death and Survival (433 genes) as the most affected pathways (Suppl. Fig. 8A-
469 C). These results are consistent with previous findings that many *Dnd1*$^{Ter/Ter}$ germ cells
470 do not enter cell cycle arrest, but are eliminated through apoptotic pathways (Cook et al.,
471 2009; Dawson et al., 2018; Yamaji et al., 2017).
472
473 **Discussion**
474
475 Germ cells are an important model to investigate how stem cells embark on a highly
476 specific differentiation pathway while restraining their potential for spontaneous
477 differentiation or tumorigenesis. While most germ cells appear to strictly control this
478 potential and successfully navigate this transition, a small subset of 129T2 *Dnd1*$^{Ter/Ter}$
479 mutant germ cells fail this test and spontaneously differentiate into teratomas - and in so
480 doing provide a tool to investigate the genetic regulation of germ cell differentiation. What
481 are the critical roles of DND1, and why does mutation in this RBP lead specifically to
482 teratoma development in a subset of mutant germ cells? To address these questions, we
483 investigated the binding targets of the DND1 protein and analyzed the transcriptome of
484 *Dnd1*$^{Ter/Ter}$ germ cells relative to wild type over the critical period following residency in
485 the gonad but prior to overt transformation. We found that DND1 down-regulates genes
486 associated with pluripotency, including multiple components of the Hippo and Bmp
487 pathways, mediates levels of many genes involved in the control of cell cycle, and is critical
488 to initiate male germ cell differentiation, which involves the activation of many chromatin
489 regulators.
490
491 DND1 is expressed from the time germ cells are allocated at the base of the allantois, and
492 as a result of its early role in germ cell development, many germ cells undergo apoptosis,
493 or are otherwise lost, prior to arrival in the gonad (Cook et al., 2009; Noguchi and
494 Noguchi, 1985). However, this transcriptome analysis reveals that overall, the

495 transcriptome of the group of mutant germ cells that survive to populate the gonad at
496 E12.5 is similar to wild type male germ cells, albeit somewhat delayed.
497
498 DND1 likely performs several roles in posttranscriptional regulation. E13.5 is a clear
499 transition point between the embryonic and fetal programs: functions of DND1 may
500 segregate into early exit from the pluripotency program, involving the degradation of
501 transcripts for many pluripotency genes, and subsequent activation of transcripts
502 associated with the male pro-spermatogonia pathway. Although we could not detect
503 pluripotency targets in HEK293 cells, Matin and co-workers previously reported *Oct4,*
504 *Nanog, Sox2, LIN28* (LIN28 family RNA-binding protein)*, Bax* (BCL2 Associated X
505 apoptosis regulator), and *Bclx* (B-cell lymphoma-estra large, apoptosis regulator) as
506 targets of DND1 in ESCs (Zhu et al., 2011). A large group of chromatin regulators mapped
507 as targets of DND1 in HEK293 cells, and all of these genes were strongly down-regulated
508 in *Dnd1*$^{Ter/Ter}$ mutants. However, it is unclear whether this down-regulation is the result
509 of post-transcriptional control or a failure to launch the male-specific differentiation
510 program.
511
512 There is strong evidence that DND1 interacts with the CNOT degradation complex, and
513 provides target specificity for NANOS2 (Suzuki et al., 2014; Yamaji et al., 2017). Because
514 *Nanos2* is not expressed in mutants, we asked whether the *Dnd1*$^{Ter/Ter}$ mutant
515 transcriptome phenocopied the *Nanos2* mutant transcriptome (Saba et al., 2014). We
516 found that many pluripotency genes showed a similar delay in down regulation during
517 the early transition (E12.5-E13.5). However, *Nanos2* mutant germ cells enter meiosis as
518 though they have lost their male identity (Suzuki and Saga, 2008), whereas *Dnd1*$^{Ter/Ter}$
519 germ cells do not. Key differences may be the up-regulation and partial compensation by
520 *Nanos3* in *Nanos2* mutants, and/or the retention of *Ret*. Neither *Nanos3* nor *Ret* is
521 expressed in *Dnd1*$^{Ter/Ter}$ germ cells.
522
523 A key finding of this study is the global identification of many chromatin regulators that
524 are activated in wild type male germ cells between E13.5-E14.5, and the observation that
525 nearly all of these fail to be activated in *Dnd1*$^{Ter/Ter}$ mutants. If the role of these chromatin
526 regulators is to stabilize the spermatogonial genome and silence somatic differentiation

527 pathways, as has often been proposed (Dawson et al., 2018; Gu et al., 2018; Heaney et al.,
528 2012), the failure to activate these genes could explain the tendency of mutant germ cells
529 to initiate differentiation to multiple cell types characteristic of teratomas. The failure to
530 activate chromatin regulators was not reported in the original *Nanos2* mutants (Saba et
531 al., 2014). However, heterozygosity for a CRISPR/*Cas9*-mediated knock out of *Nanos2*
532 on the 129/SvJ background led to a decrease in DNMT3L expression, a defect in re-
533 methylation of the male germ cell genome, elevated levels of *Line-1*, and an increase in
534 teratoma incidence (Dawson et al., 2018).
535
536 Many genes associated with the cell cycle are targets of DND1 and are dysregulated in
537 mutants (this study;(Cook et al., 2011; Yamaji et al., 2017). Several signaling pathways,
538 including Kit, Fgf, Nodal, and Hippo are also elevated and could be responsible for driving
539 ongoing proliferation. The association of FOXH1 with the YAP/SMAD complex is believed
540 to drive the switch from pluripotency to differentiation of mesendoderm (Slagle et al.,
541 2011), but further studies would be required to determine whether this finding has
542 relevance for the differentiation of cell types in teratomas. A failure to exit active cell cycle
543 and enter G0 arrest is a characteristic of mutant germ cells and teratoma formation, but
544 whether this failure is causal remains unclear.
545
546 Based on the failure to activate many repressors of transposable elements such as *Piwil4,*
547 *Morc1, Mael*, and *Tdrd5*, we anticipated a strong activation of LINES and other
548 transposons. However, at the latest stage of our analysis (E14.5), we did not detect
549 significant changes in this category. Similarly, despite the absence of many epigenetic
550 regulators that normally characterize the male germ cell transcriptome at these stages, we
551 found no evidence of lineage infidelity. One possibility is that E14.5 (the latest stage of
552 this analysis) is too early to detect these changes at the population level. There is
553 significant variability in the response of individual germ cells to the *Dnd1*^{Ter} mutation.
554 *Dnd1*^{Ter} mutant germ cells transform and form teratomas at a much higher rate than
555 wildtype germ cells. However, even though the "per mouse" teratoma rate is high, the
556 "per germ cell" transformation rate is still quite low. Most *Dnd1*$^{Ter/Ter}$ germ cells undergo
557 apoptosis, as evidenced by the strong footprint of cell death and cell cycle disruption at
558 the population level. A molecular explanation for this cell heterogeneity remains elusive.

559

560 For stem cell biology, it would be very instructive to know the steps involved in the
561 transition from a germ cell to a teratoma. Dawson and colleagues have recently suggested
562 that this involves a transition through a primed pluripotent EC cell state (Dawson, 2018).
563 The fact that only a few germ cells form teratomas in a *Dnd1*$^{Ter/Ter}$ testis, while other germ
564 cells nearby either die or continue to express normal germ cell markers (Cook et al., 2011;
565 Dawson et al., 2018), suggests that the trigger must be a threshold event that is influenced
566 by cell autonomous fluctuations of factors in germ cells and/or by the microenvironment
567 in the testis of some strains. Teratoma formation likely competes with apoptotic pathways
568 that are strongly activated at all stages of our analysis. In this study, we have identified
569 many targets of DND1 and captured their transcriptional changes in *Dnd1*$^{Ter/Ter}$ germ
570 cells. However, the specific transcriptional events in the rare cells undergoing the
571 transition to teratoma may be obscured by the transcriptomes of the large number of cells
572 that are not. We plan to use a single cell analysis in future experiments to resolve this
573 problem.
574

575 **Acknowledgments**

576 We would like to thank the teams in the FACS and Genomics Cores at Duke, especially
577 Mike Cook, Nicolas Devos, and Olivier Fedrigo, who helped with these experiments and
578 their analysis. We are also grateful to Alex Bortvin, who provided information for the
579 RepEnrich analysis, to Joe Nadeau, who supplied the mice that founded our *Dnd1*^{Ter}
580 colony, and to past and present members of the Capel lab, especially Jordan Batchvarov,
581 who contributed to the management of the strain over the last 10 years and Mike
582 Czerwinski, who transferred bioinformatics expertise to JG. This work was funded by a
583 grant to BC from NIH (GM087500), Bridge Funding from DUMC, and a grant to JK from
584 NCI (CA157268) and Bridge Funding from DUMC.

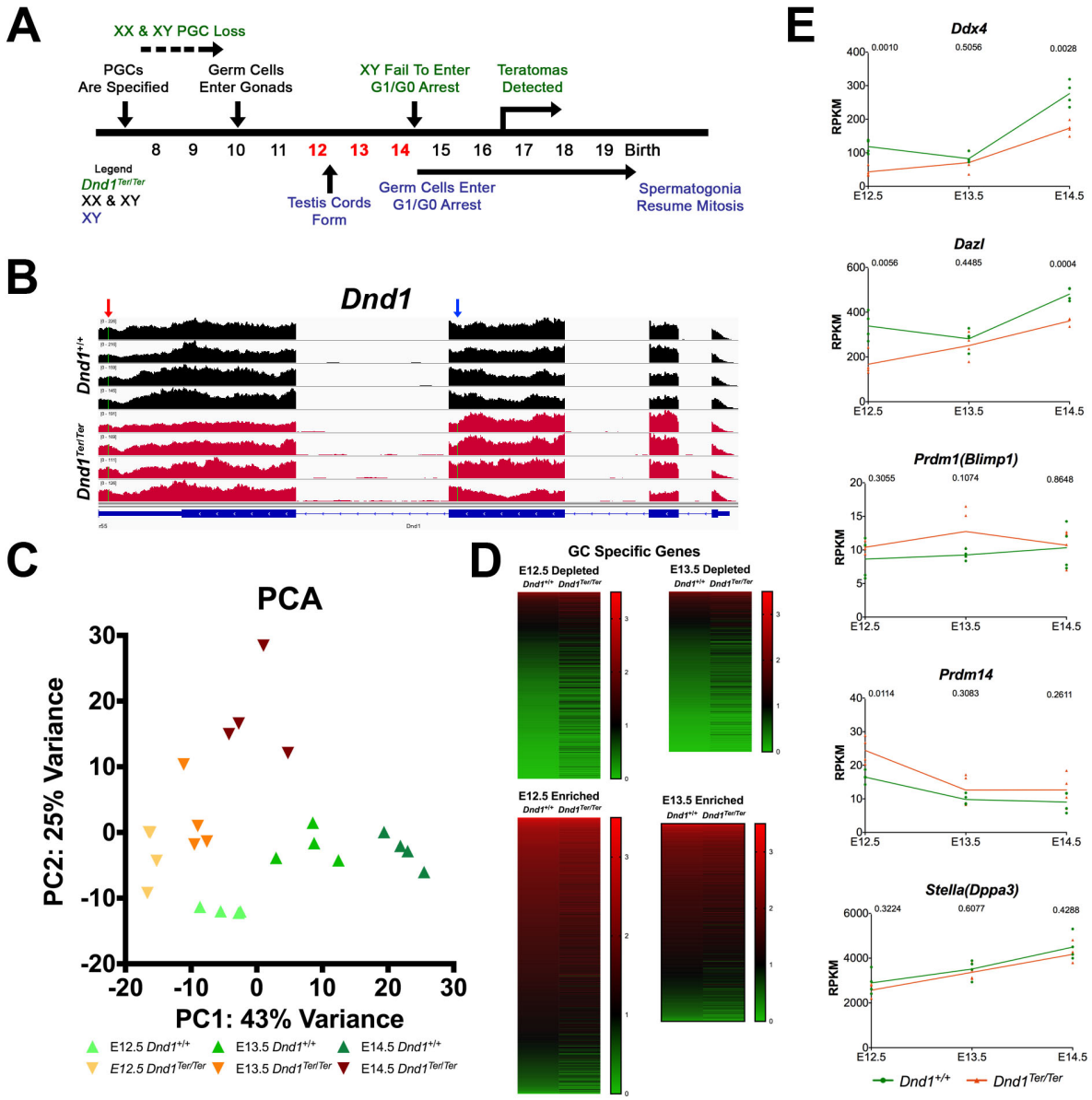

Figure 1. Male germ cells in *Dnd1*$^{Ter/Ter}$ mutants retain a germ cell identity. (A) Time line of male germ cell development and defects in *Dnd1*$^{Ter/Ter}$ mutants. Primordial germ cells (PGCs) are specified at ~E7.5, migrate and arrive in the gonad at E10.5. In the male gonad, they are enclosed inside testis cords by E12.5, and undergo G0 arrest between E14.5-E15.5, remaining in arrest until after birth. In *Dnd1*$^{Ter/Ter}$ mutants, many PGCs are lost soon after specification. Remaining germ cells enter the gonad, but fail to arrest in G0. Teratomas are detected in the fetal testis beginning at ~E16.5 (shown

in green above time line). **(B)** *Dnd1* is transcribed in mutants similar to wild type levels at E12.5. The *Ter* mutation is visible in the 2nd exon of all mutant samples (blue arrow, red samples), whereas the 129T2-specific SNP (red arrow) is present in all samples in the 5' non-coding region. **(C)** A PCA analysis revealed that mutant germ cells are more similar to wild type at E12.5 and E13.5 and diverge further at E14.5. **(D)** Nonetheless, male germ cells show an overall expression pattern characteristic of germ cells with respect to genes that are normally depleted (top) and genes that are normally up-regulated (bottom) at E12.5 and E13.5. **(E)**. Specific examples of gene expression across the timecourse (green line = wild type samples; orange line = *Dnd1*$^{Ter/Ter}$ in all graphs in the manuscript; significance values for each time point are shown at top of graph). While both *Ddx4* (*Vasa*) and *Dazl* show a delay in activation, similar levels at E13.5, and a slight down regulation at E14.5, *Prdm1* (*Blimp1*), *Prdm14*, and *Stella (Dppa3)* show no significant differences from wild type at any stage.

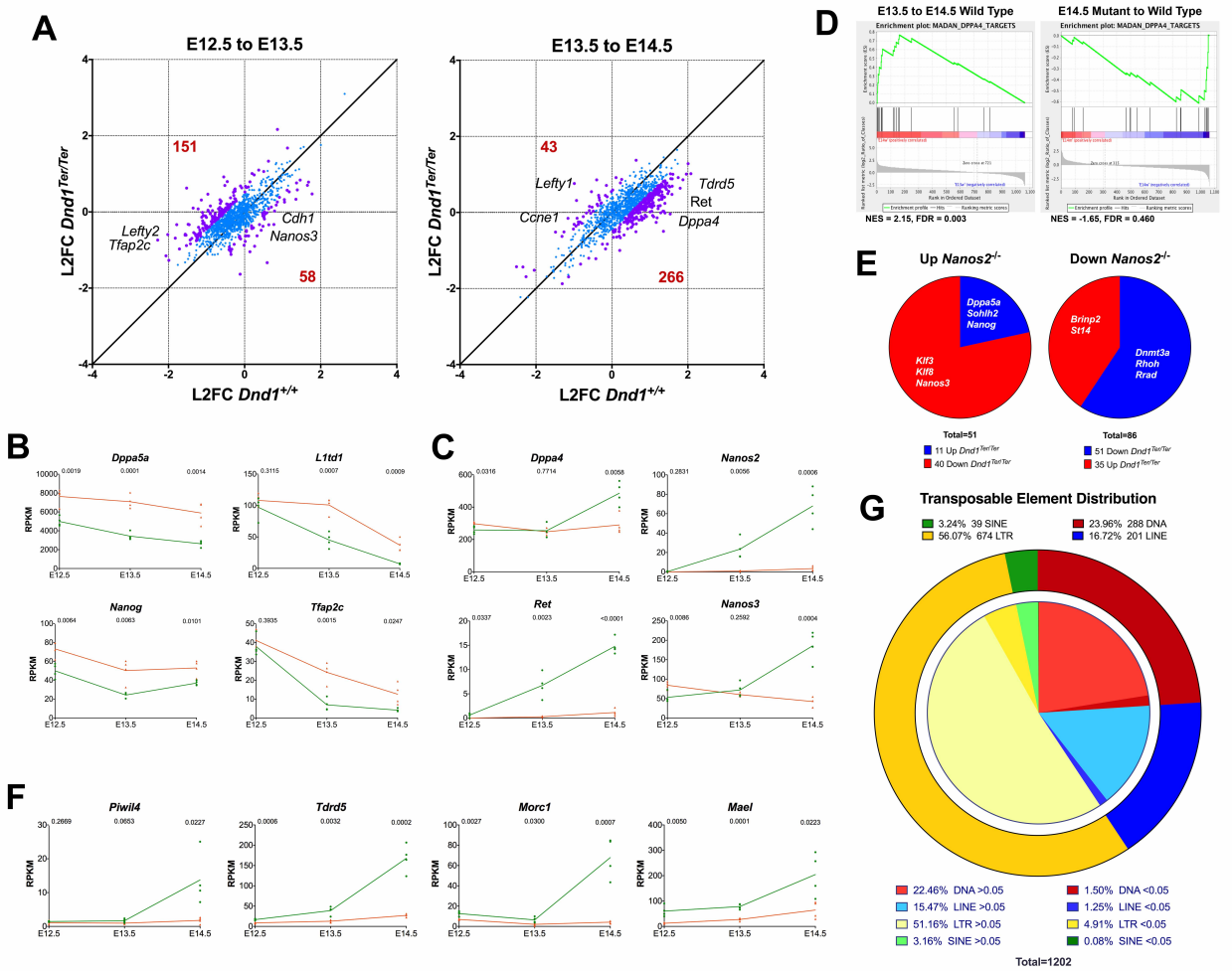

Figure 2. *Dnd1*$^{Ter/Ter}$ mutant germ cells show delayed suppression of pluripotency, and a failure to activate the male differentiation program. (A) Scatter plots illustrating dynamic changes in expression of germ cell specific genes (data from Jameson et al., 2012) between mutant (Y axis) and wild type (X axis) during the transitions between E12.5-E13.5 and E13.5-E14.5. Between E12.5-E13.5 more genes (151) show a higher $\log_2$ fold change (L2FC) in mutants than in wild type, while only 58 genes lag behind. In the transition between E13.5-E14.5, the reverse is true: more genes lag behind wild type expression (266). Of the 43 genes that show a higher L2FC in this interval, many belong to cell cycle or elevated signaling pathways. Points with L2FC between mutant and wild type >0.5 in purple, <0.5 in blue. **(B)** Examples of 4 genes associated with pluripotency (*Dppa5a*, *L1td1*, *Nanog*, and *Tfap2c*) that show a delay in down-regulation in *Dnd1*$^{Ter/Ter}$ mutant germ cells. **(C)** Examples of 4 genes associated

with initiation of the male pathway (*Dppa4, Nanos2*, *Ret*, and *Nanos3*) that fail to be activated. **(D)** Consistent with this, based on GSEA analysis, targets of *Dppa4* are not enriched in mutant germ cells during the E13.5-E14.5 transition. **(E)** Some transcriptional changes in *Nanos2* mutants are discordant with changes in *Dnd1*$^{Ter/Ter}$ mutants. Of genes up in *Nanos2* mutants, 11 behave the same (blue) and 40 (red) are down in *Dnd1*$^{Ter/Ter}$. Of genes down in Nanos2 mutants, 51 are also down in *Dnd1*$^{Ter/Ter}$ (blue) and 35 are up (red)(Saba et al., 2014). Only genes with significant L2FC are shown ($p<0.05$). See also Suppl. Table 3. **(F)** Examples of genes associated with suppression of transposable elements and the piRNA pathway activated in wild type but not mutants. **(G)** Although many silencers of repetitive elements were down-regulated, RepEnrich analysis showed that transposable elements did not exhibit significant aberrant activity at E14.5. Transposable element distribution organized by class: Outer ring: class distribution of elements represented in reads at E14.5 (yellow=LTRs; green=SINEs; Red=DNA transposons; Blue=LINEs). Inner circle divides specific classes into reads with significant differences between mutant and wildtype (bold colors: FDR<0.05; pale colors: FDR>0.05).

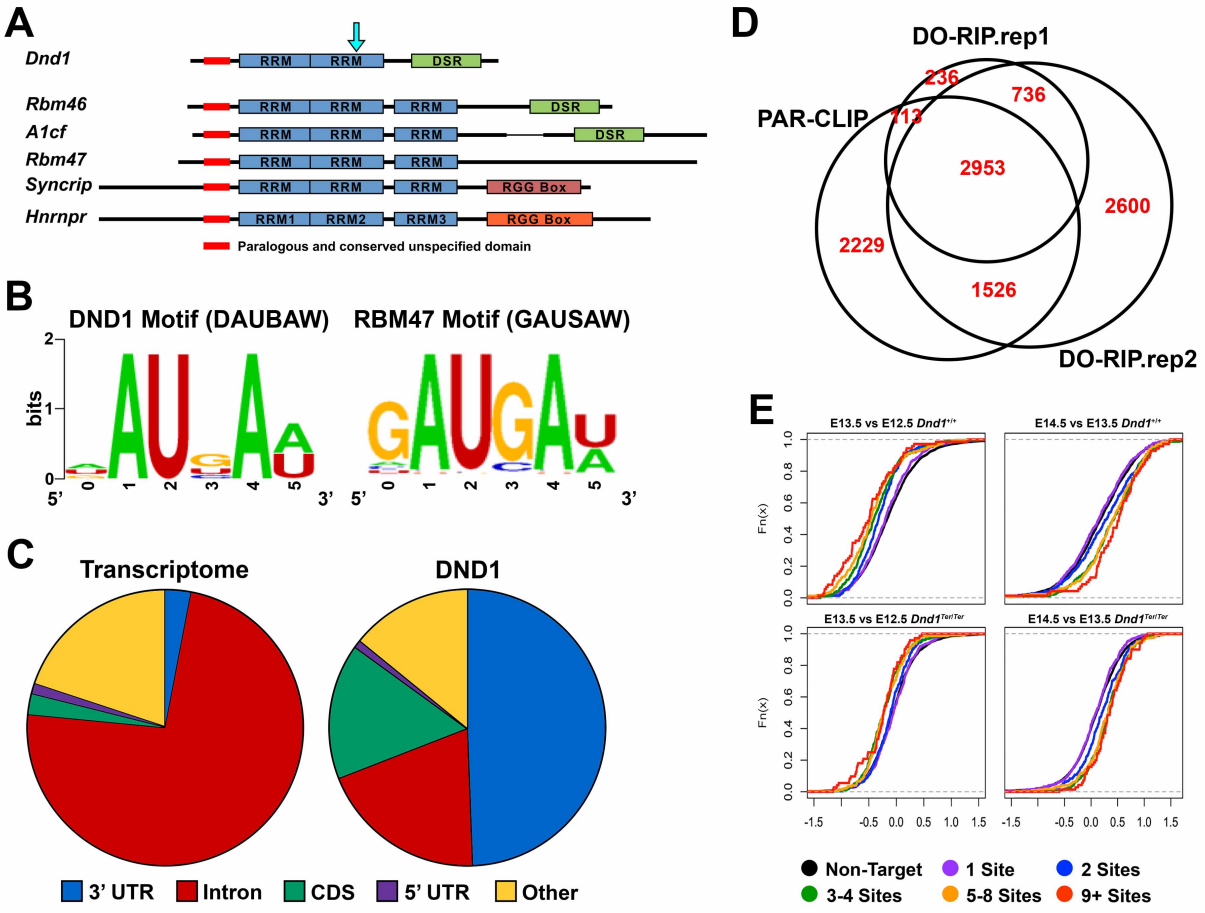

Figure 3. DND1 binds to the DATBAW motif preferentially localized to 3' UTRs, and regulates the up- and down-regulation of targets. (A) DND1 and five other RBPs (RBM46, A1CF, RBM47, SYNCRIP and HNRNPR) are part of a subfamily containing RNA recognition motifs (RRMs) sharing sequence similarity. Three of these subfamily member (DND1 included) also have similar C-terminal double stranded RNA binding domains (DSR) The black arrow indicates the position of the Ter mutation, partially truncating the second RRM and completely removing the DSR. **(B)** k-mer analysis was preformed to identify the most enriched motif in Dnd1 DO-RIP-Seq binding sites (http://weblogo.berkeley.edu), this motif is highly similar to a previously identified motif of a related RBP, Rbm47 (Ray et al., 2013). **(C)** The locations of DND1 binding sites were broken down into regions (3'UTR, intron, CDS, 5'UTR, and other) and compared to the proportion of the regions present in the expressed transcriptome. DND1 has a strong preference for binding 3'UTR sequences and a slightly weaker preference for coding

sequence (CDS). **(D)** Comparison of DND1 binding sites identified in the two replicates of the present study and binding sites identified by PAR-CLIP in Yamaji et al., 2017 (Yamaji et al., 2017)**(E)** Cumulative distribution function (CDF) plots evaluating RNA abundance under four conditions (E12.5-E13.5, and E13.5-E14.5 in both mutant and wild type germ cells) with changes for transcripts classified by the number of DND1 binding sites (non-targets, 1 site, 2 sites, etc). In wild type germ cells RNA abundance of DND1 targets is more likely to decrease between E12.5 and E13.5 than for non-targets. In contrast, between 13.5 and 14.5 RNA abundance of DND1 targets generally increases. The effects are amplified by increasing the number of DND1 binding sites. In *Dnd1* mutant germ cells, RNA abundance changes for both E12.5-E13.5 and E13.5-E14.5 are similar for DND1 targets and non-targets.

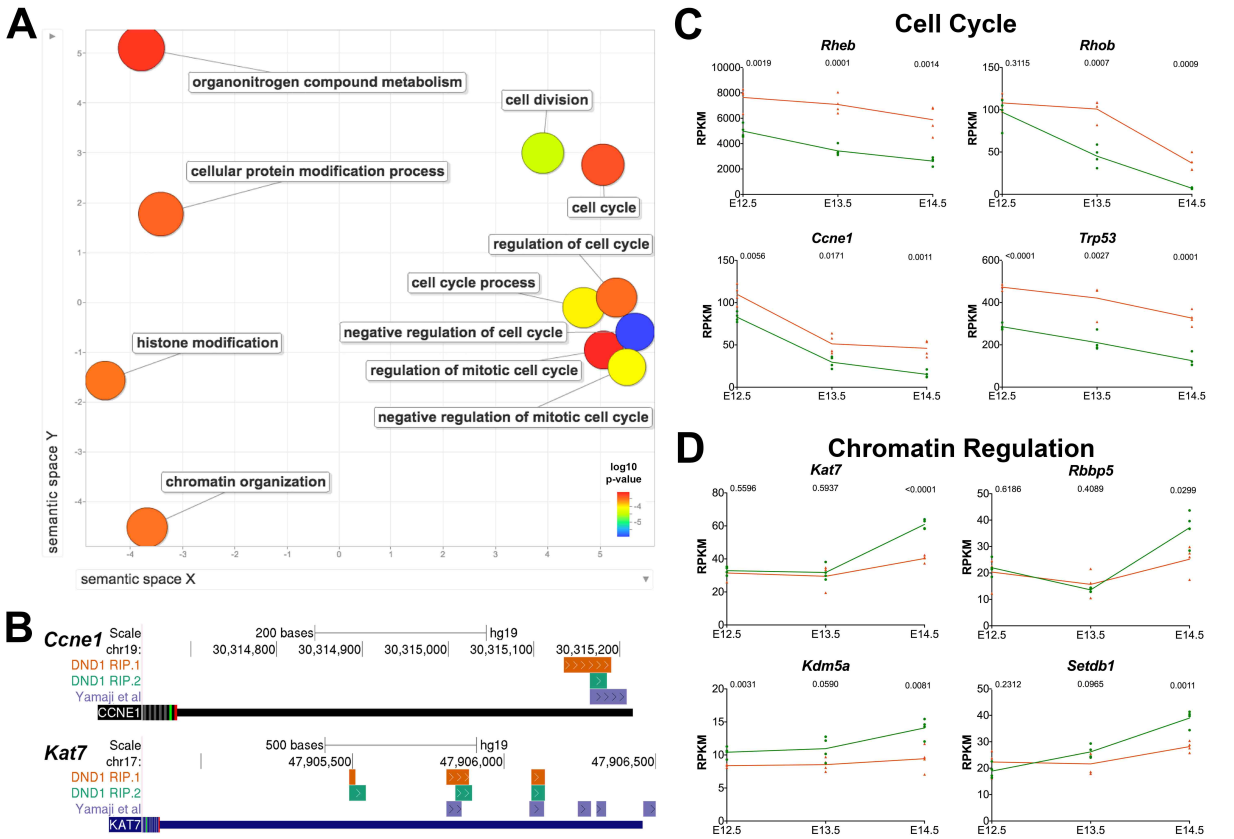

Figure 4. DND1 targets include cell cycle genes and chromatin regulators, which are both up and down-regulated in mutant germ cells. (A) Semantic similarity clustering of GO terms enriched in DND1 DO-RIP-seq targets indicated that the most common categories of targets of DND1 are genes associated with cell cycle and chromatin regulation. **(B)** Two examples of DND1 targets, *Ccne1* and *Kat7*. Binding sites for DND1 are present in the 3'UTR of *Ccne1* and *Kat7* in both DO-RIP-seq experiments and in the Yamaji dataset (Yamaji et al., 2017). **(C)** Examples of cell cycle gene targets that are up-regulated in mutants at E14.5 (*Rheb*, *Rhob*, *Ccne1*, and *Trp53*). **(D)** Examples of chromatin regulators that are down-regulated in mutants relative to wild type by E14.5 (*Kat7*, *Rbbp5*, *Kdm5a*, and *Setdb1*).

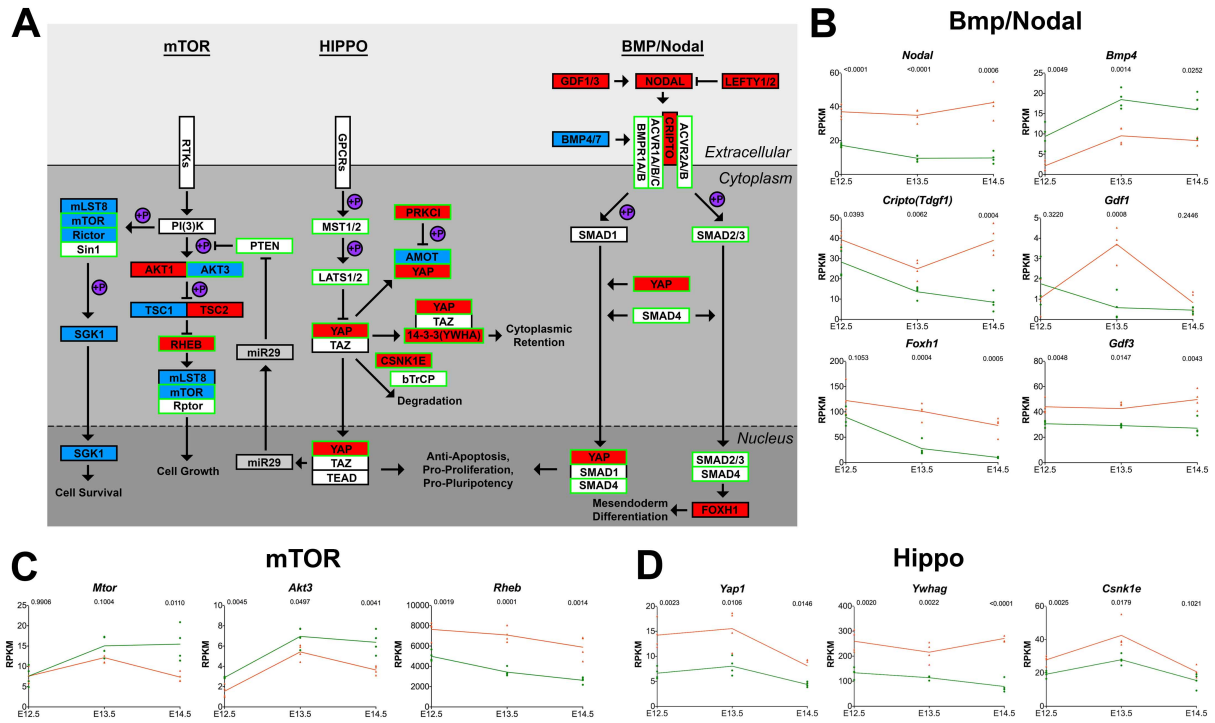

Figure 5. In the presence of the *Ter* mutation in *Dnd1*, members of mTOR, Hippo and Bmp/Nodal pathways have altered expression with some transcripts indicated as direct targets of DND1. (A) Interactions for mTOR, Hippo, and BMP/Nodal signaling pathways based primarily on KEGG analysis (Kanehisa et al., 2017) with input from primary literature (Beyer et al., 2013; Fuerer et al., 2014; Shimobayashi and Hall, 2014; Slagle et al., 2011; Spiller et al., 2017; Tanaka et al., 2007; Yu and Guan, 2013). Genes in pathways showing altered expression are colored blue for depression and red for elevation (RNAseq). Genes that map as transcript targets of DND1 based on RIP/ RIPseq are boxed in green. **(B,C,D)** Graphs for representative genes in pathways. **(B)** *Nodal*, *Cripto*, *Foxh1*, and *Gdf3* show strong up-regulation while *Bmp4* is down-regulated in the mutant transcriptome data. *Gdf1* has a spike in up-regulation after E12.5. **(C)** Genes mapping as DND1 targets in the mTor pathway including *Mtor* and *Akt3* are down-regulated while the target *Rheb* is strongly up-regulated in mutants. **(D)** Genes in the Hippo pathway, including *Yap1*, *Ywhag,* and *Csnk1e* are targets of DND1 that are up-regulated in mutants.

Supplemental Figure Legends

Suppl. Table 1. RNAseq gene expression graphing. We provide an excel file with **(A)** the RPKM values used in our analysis and **(B)** the graphic format used to display gene expression in wild type and *Dnd1*$^{Ter/Ter}$ mutants over time. The user can copy any from **(A)** with values into row 2 of **(B)** to generate the graph for that gene.

Suppl. Table 2. The list of changed genes defined by GSEA as part of the "DPPA4 Targets".

Suppl. Table 3. List of genes that are **(A)** up-regulated or **(B)** down-regulated in *Nanos2* mutants, annotated for activity in *Dnd1*$^{Ter/Ter}$ mutants.

Suppl. Table 4. (A) List of all genes (expressed or not expressed in HEK293 cells), indicating genes identified in DO-RIP and/or PAR-CLIP (Yamaji et al., 2017). **(B)** List of all binding sites enriched in DO-RIP-seq. **(C)** List of genes with reproducible 3'UTR binding sites enriched in both DO-RIP-seq experiments. This table was used to label targets in Figure 5A.

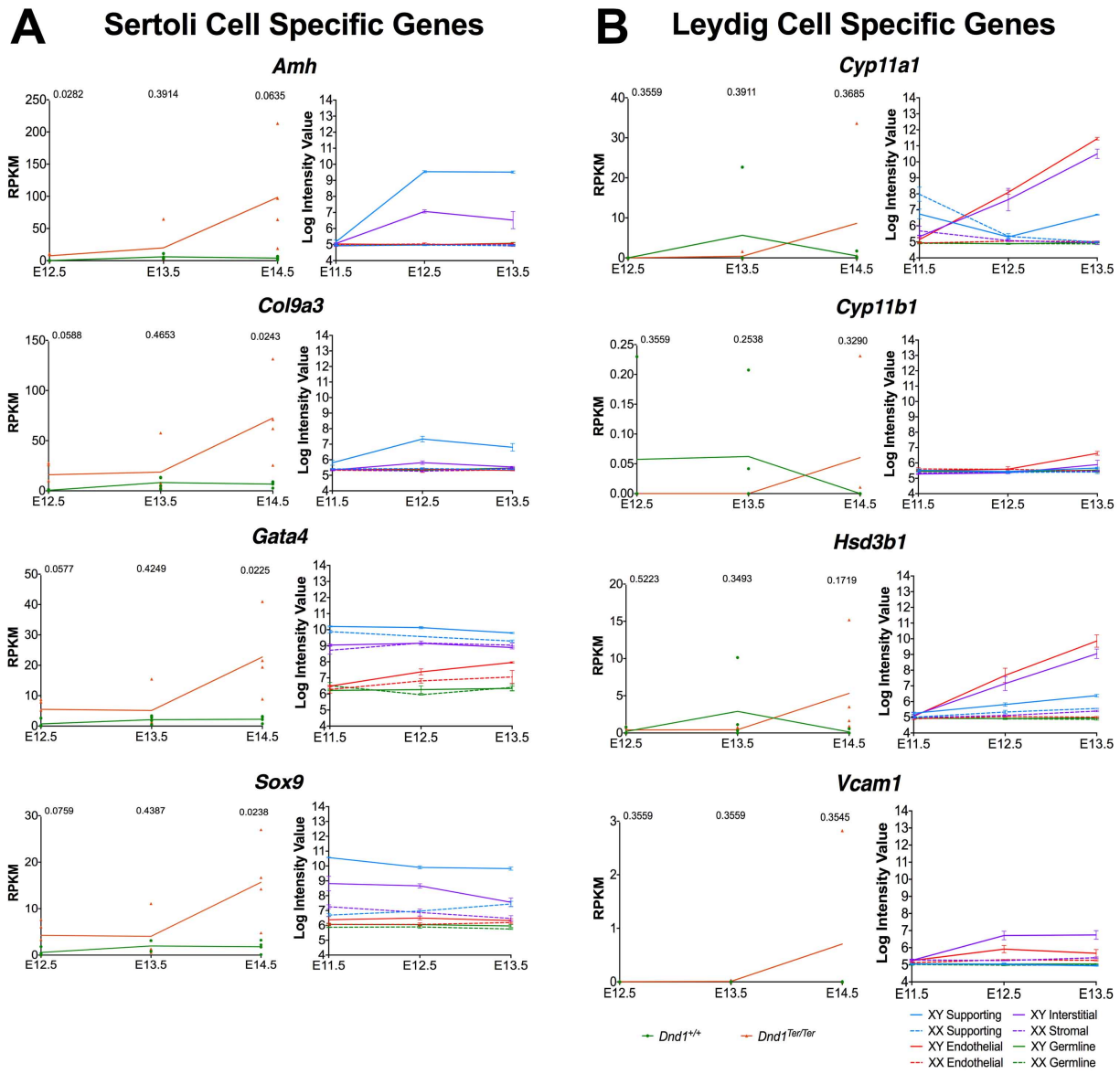

Suppl. Fig. 1. Examples of genes detected in the *Dnd1*$^{Ter/Ter}$ transcriptome data that are specific to Sertoli or Leydig cell lineages in the gonad based on the Jameson data (Jameson et al., 2012). Typically, expression of these genes spikes in the E14.5 *Dnd1*$^{Ter/Ter}$ data, a stage when *Dnd1*$^{Ter/Ter}$ germ cell numbers are reduced and expression of Oct4-GFP declines, which may have led to errors in threshold settings during FACS. Graphs of transcriptome data from each cell type in the gonad performed at E11.5, E12.5 and E13.5 are shown for comparison. The germ cell lineage is green; supporting cells are blue; interstitial/stromal cells are purple; endothelial cells are red.

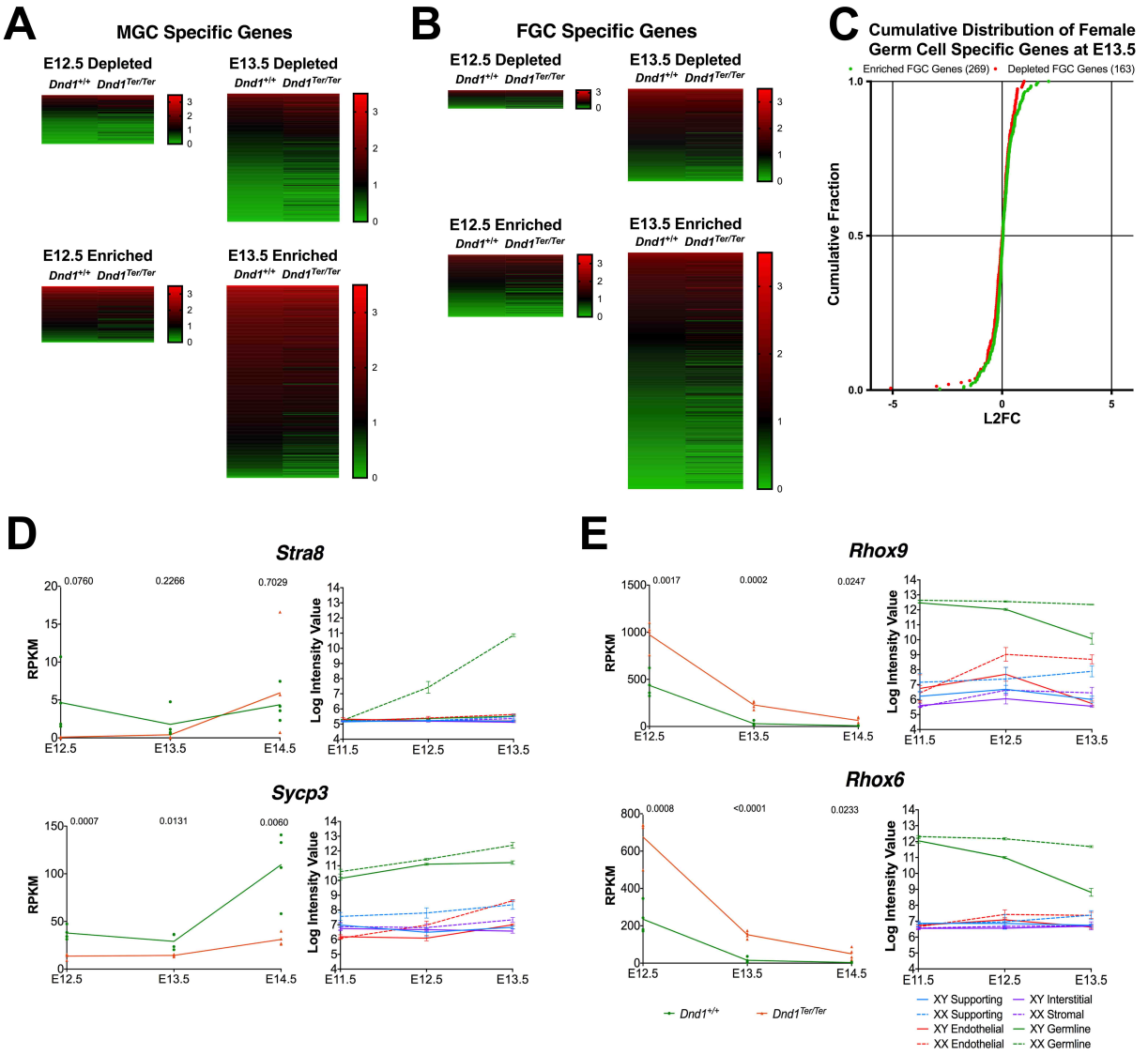

Suppl. Fig. 2. Male germ cells do not acquire a female (or meiotic) identity, but retain expression of pluripotency genes shared with female germ cells. **(A)** Heat map analysis showing that *Dnd1*$^{Ter/Ter}$ male germ cells retain a profile very similar to wild type at E12.5 and E13.5 with respect to genes that are specifically depleted in male germ cells, and genes that are specifically enriched. **(B)** Similarly, heat maps comparing expression of female-specific genes in XY *Dnd1*$^{+/+}$ to XY *Dnd1*$^{Ter/Ter}$ samples show few changes for depleted or enriched genes at E12.5 or E13.5. **(C)** A cumulative distribution plot of the log2 fold change between mutant male germ cells and wild type male germ cells at E13.5 for female germ cell enriched (green) or depleted (red) genes. Genes typically enriched (green) or depleted (red) in female germ cells show no clear bias

for the direction of change in mutant germ cells. **(D)** Genes specifically upregulated as female germ cells enter meiosis (*Stra8* and *Sycp3*) were not activated by E14.5 in *Dnd1*$^{Ter/Ter}$ mutants. Graphs to the left show expression of the gene in all gonadal lineages (green broken line = XX germ cells; green solid line = XY germ cells; data from Jameson et al., 2012). **(E)** *Rhox9* and *Rhox6*, which normally become specific to XX germ cells by abrupt down-regulation in male germ cells, show a delay in down-regulation similar to other pluripotency genes.

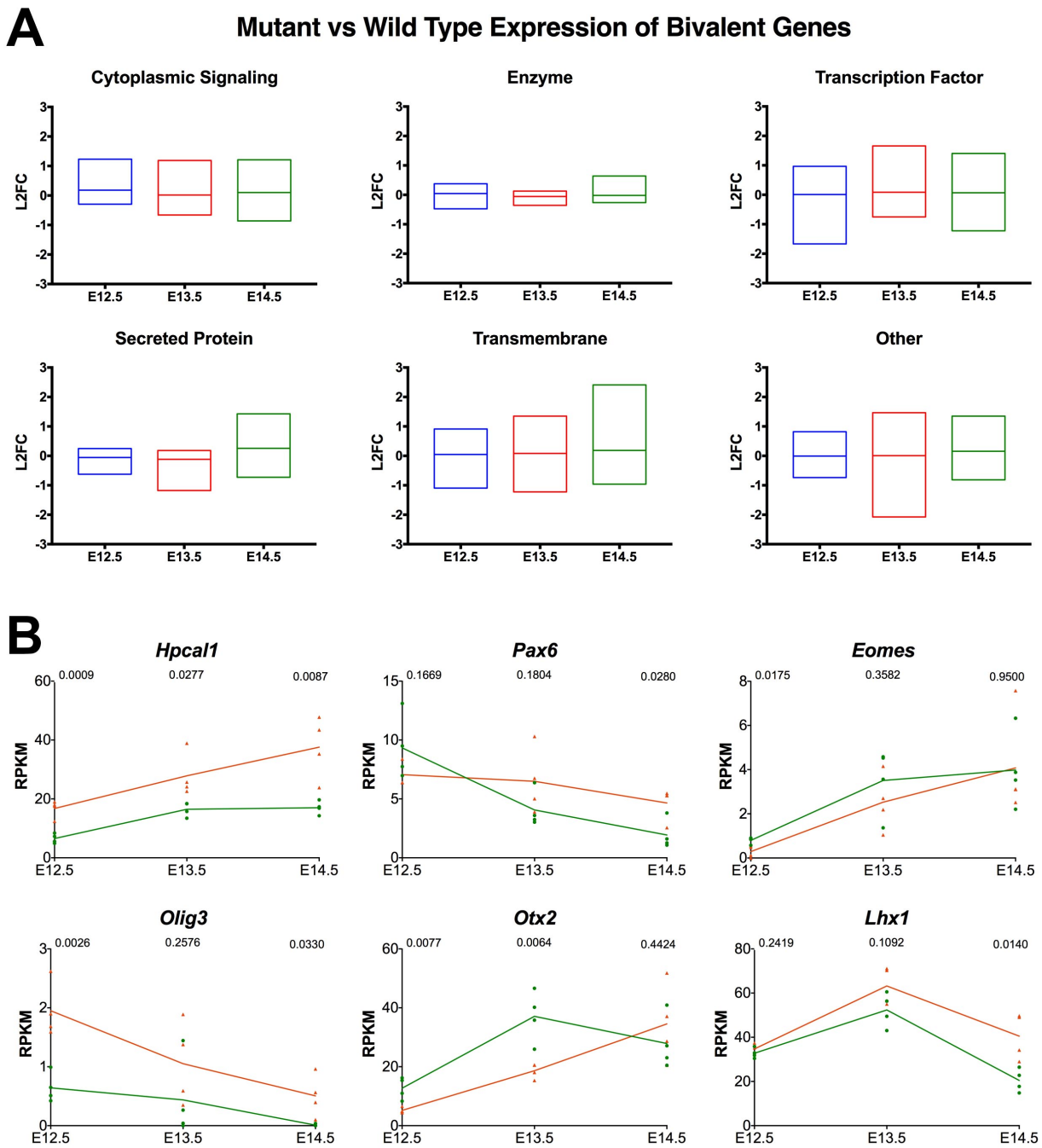

Suppl. Fig. 3. *Dnd1*$^{Ter/Ter}$ germ cells show no evidence of lineage infidelity between E12.5-E14.5. Despite the failure to activate many chromatin regulators in *Dnd1*$^{Ter/Ter}$ mutants, **(A)** expression of bivalent genes grouped by category (cytoplasmic signaling proteins, enzymes, transcription factors, secreted proteins, transmembrane proteins, and other) was not elevated, and **(B)** with the exception of *Hpcal1,* neither neuronal genes, nor other transcription factors associated with somatic cell

differentiation (*Pax6*, *Eomes*, *Olig3*, *Otx2*, and *Lhx1*) were significantly elevated in mutants.

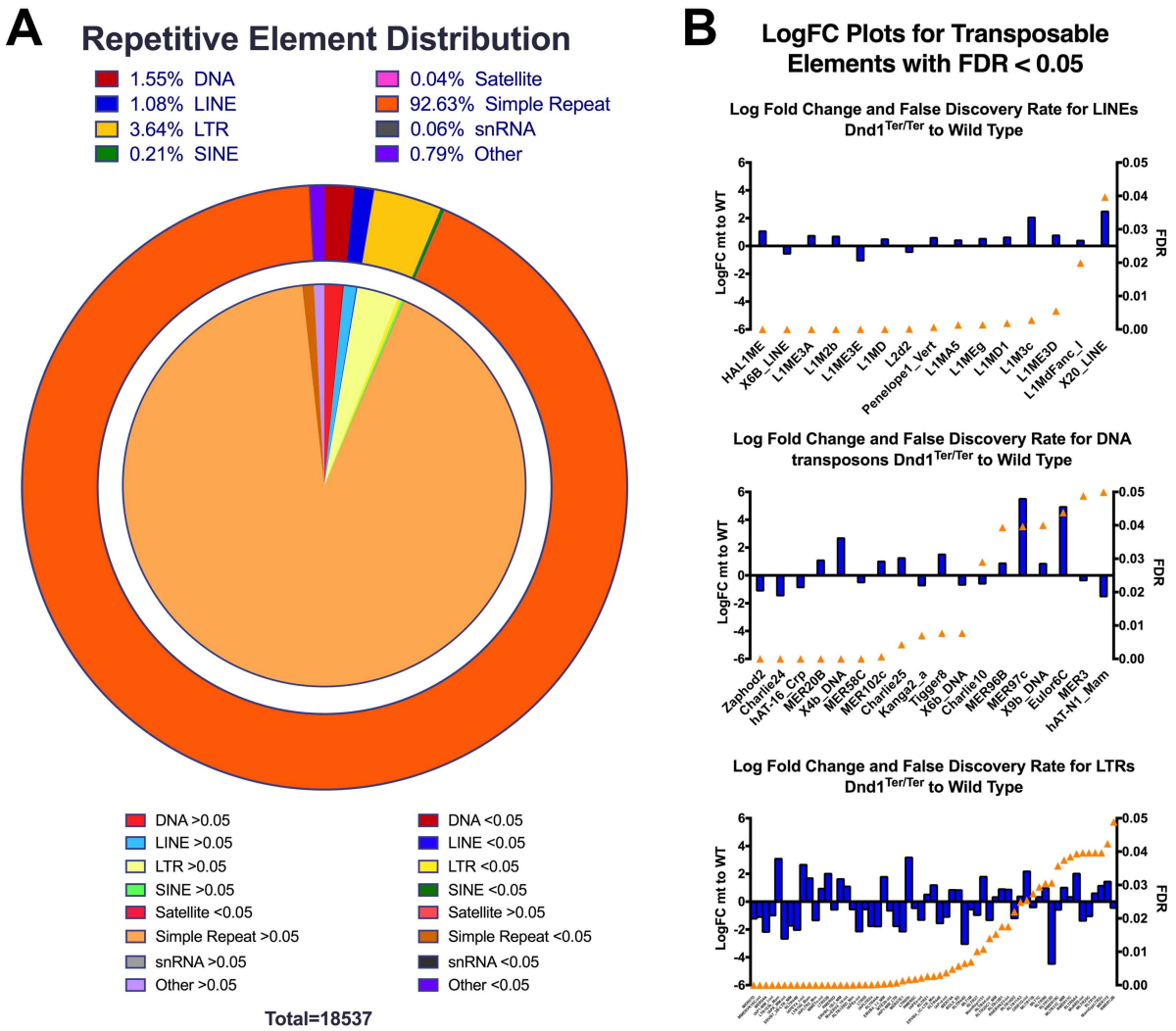

Suppl. Fig. 4. Repetitive elements in general do not exhibit aberrant activity. **(A)** A survey of repetitive element distribution organized by class. Outer ring: class distribution of elements represented in reads at E14.5 (Red=DNA transposons; Blue=LINEs; gold=LTRs; green=SINEs; Magenta=satellite; Orange=simple repeats; Dark Green=snRNAs; Purple=other). Inner circle divides specific classes into reads with significant differences between mutant and wildtype and reads without significant differences between mutant and wildtype (bold colors: FDR<0.05, significant; pale colors: FDR>0.05). **(B)** Waterfall plots of Log Fold Change (LogFC) between mutant and wildtype in each transposable element class (LINEs, LTRs, and DNA transposons) with

FDR<0.05 (significant). LogFC shown to left of plots; FDR shown by orange triangle placement relative to right scale on each graph.

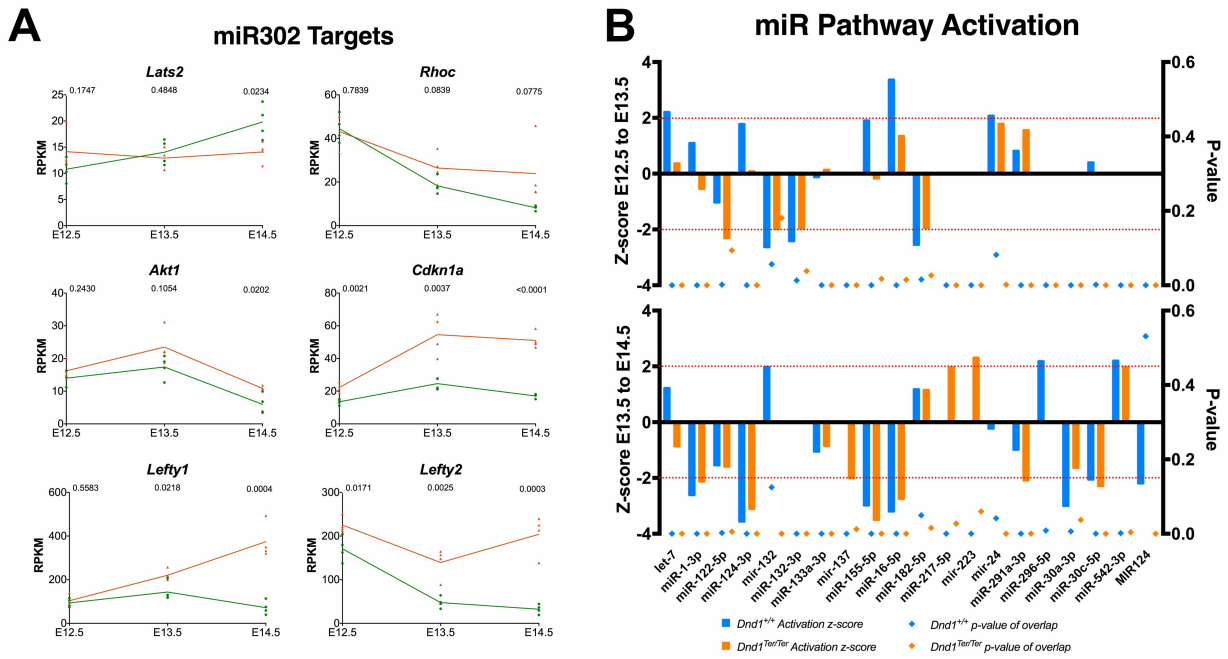

Suppl. Fig. 5. In general, miRNAs did not show activation based on downstream target analysis. (A) Although DND1 is believed to block degradation of zebrafish miR430 targets, with the exception of *Lats2*, targets of the orthologous miRNA in mice (miR320) are not down-regulated in mutants as predicted. **(B)** Waterfall graphs of Ingenuity Pathway Analysis (Qiagen) of miRNA activation based on expression changes in predicted targets at E12.5-E13.5 (top) and E13.5-E14.5 (bottom) for wild type (blue) and mutant (orange) samples. Only miRNA pathways with an activation Z-score of >2 or <-2 (left y-axis) in at least one transition period for mutant or wild type data are shown. P-values are plotted on the right Y-axis and represented as diamonds.

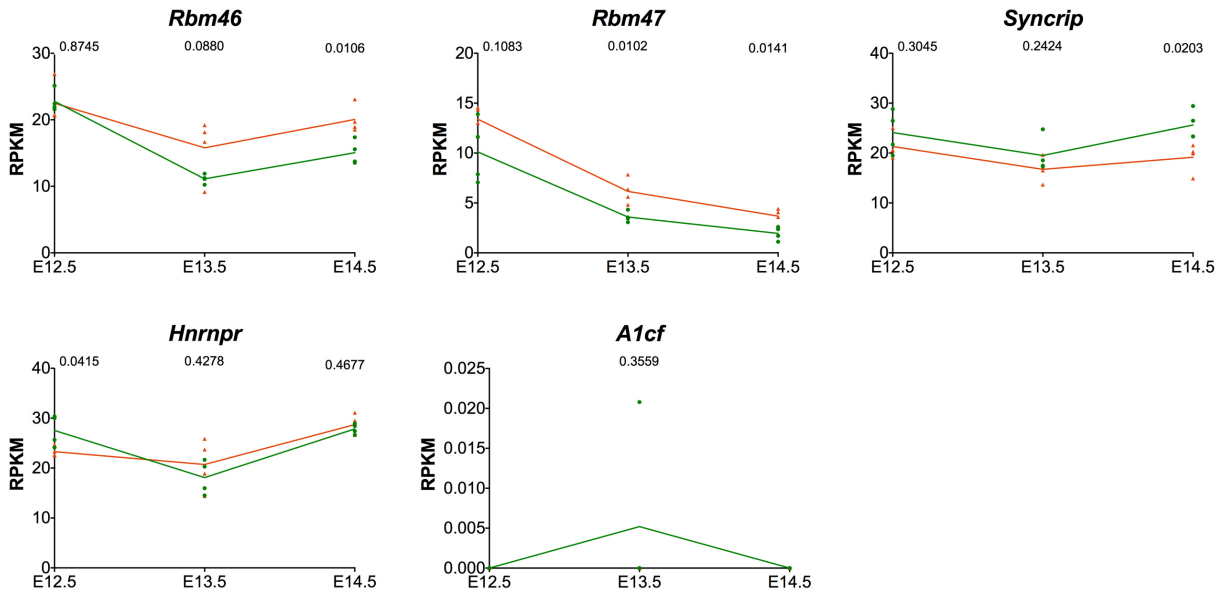

Suppl. Fig 6. Four RBPS closely related to DND1 are expressed in germ cells. Four of the five RNA binding proteins (*Rbm47*, *Rbm46*, *Syncrip*, *Hnrnpr*, but not *A1cf*) related to DND1 (Fig. 3) are expressed in male germ cells during the transcriptome timecourse.

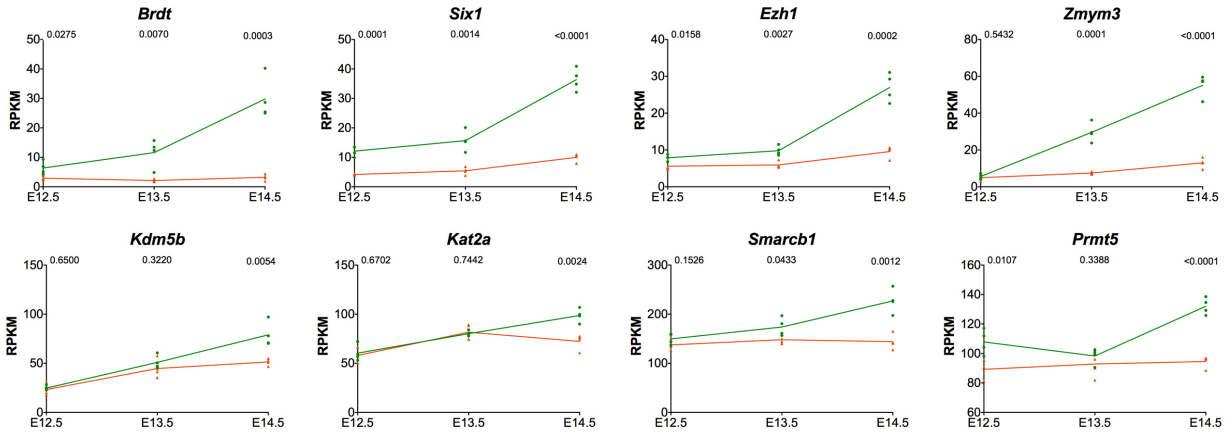

Suppl. Fig. 7. Many chromatin regulators that are not expressed in HEK293 cells, thus did not map as targets of DND1, fail to be activated in mutants. Nine additional chromatin regulators (*Brdt*, *Six1*, *Ezh1*, *Zmym3*, *Kdm5b*, *Kat2a*, *Smarcb1*, and *Prmt5*) are all expressed at lower levels in *Dnd1*$^{Ter/Ter}$ mutants likely reflecting a failure to activate the male pathway.

A

Pathway	P-value	# Affected Genes
Cell Death and Survival	$1.05E^{-04} – 3.21E^{-22}$	433
Cellular Growth and Proliferation	$1.06E^{-04} – 5.18E^{-20}$	482

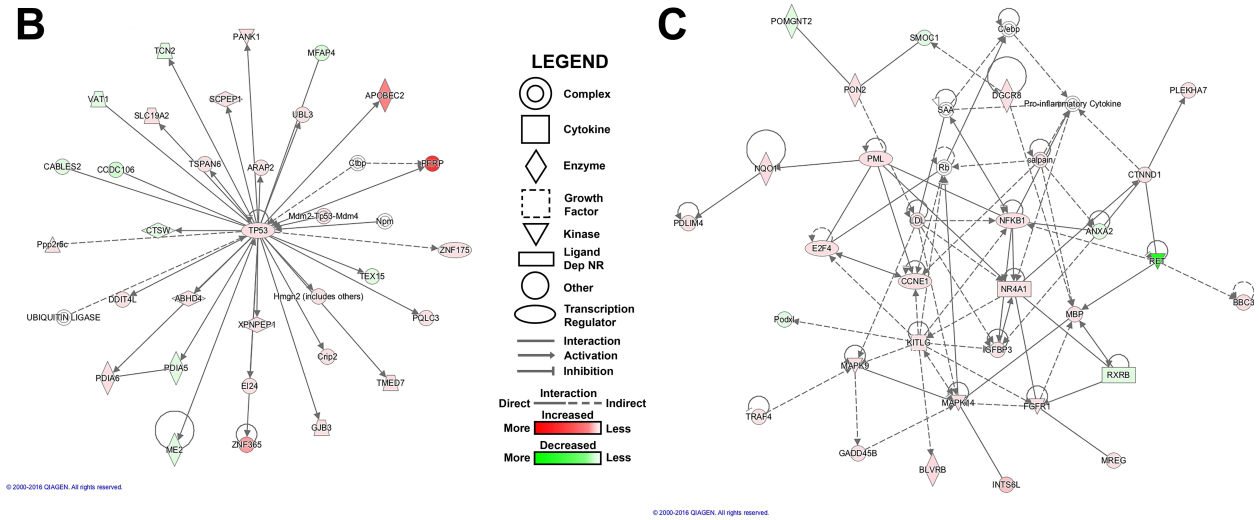

Suppl. Fig. 8. Cell death and cell cycle pathways are strongly affected in *Dnd1*$^{Ter/Ter}$ mutants. (A) Ingenuity pathway analysis identified cell death (433 genes) and cell cycle (482 genes) pathways as the most strongly affected in *Dnd1*$^{Ter/Ter}$ mutants. **(B)** Network diagram centered on *Tp53*, depicting the relationship of many cell death and survival genes. **(C)** Network diagram centered on *Ccne1*, depicting the relationship of many cell cycle genes, most of which are up-regulated.

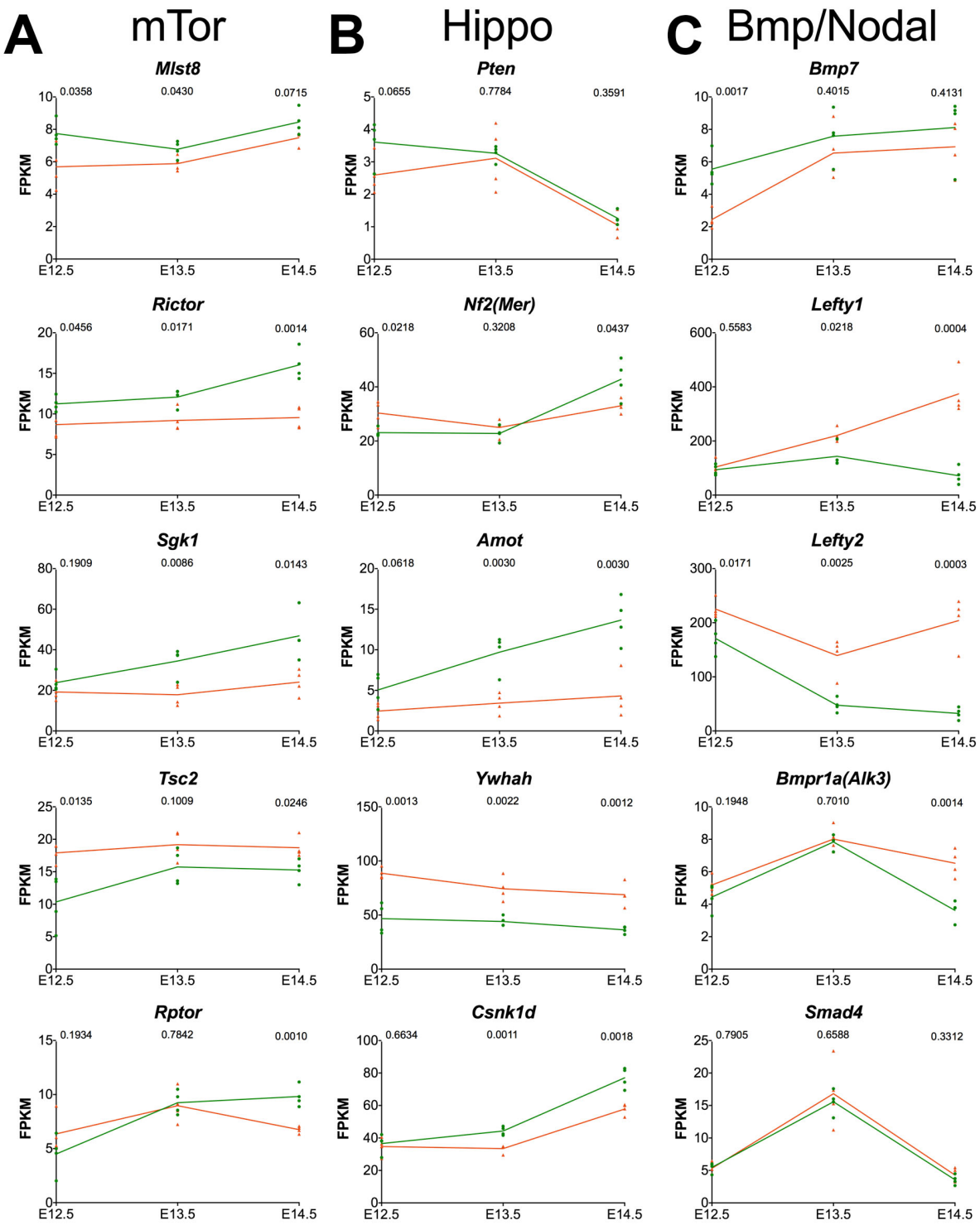

Suppl. Fig. 9. Expression of genes in the mTor, Hippo and Bmp/Nodal pathways are altered in *Dnd1*$^{Ter/Ter}$ mutants. Expression of other members of the **(A)** mTor, **(B)** Hippo and **(C)** Bmp/Nodal pathways from Fig. 5 is misregulated in mutants with some mapping as transcript targets of DND1 (Fig. 5A).

REFERENCES

Beyer, T.A., Weiss, A., Khomchuk, Y., Huang, K., Ogunjimi, A.A., Varelas, X., Wrana, J.L., 2013. Switch enhancers interpret TGF-beta and Hippo signaling to control cell fate in human embryonic stem cells. Cell reports 5, 1611-1624.

Bhattacharya, C., Aggarwal, S., Kumar, M., Ali, A., Matin, A., 2008. Mouse apolipoprotein B editing complex 3 (APOBEC3) is expressed in germ cells and interacts with dead-end (DND1). PloS one 3, e2315.

Bustamante-Marin, X., Garness, J.A., Capel, B., 2013. Testicular teratomas: an intersection of pluripotency, differentiation and cancer biology. The International journal of developmental biology 57, 201-210.

Ciosk, R., DePalma, M., Priess, J.R., 2006. Translational regulators maintain totipotency in the Caenorhabditis elegans germline. Science 311, 851-853.

Cook, M.S., Coveney, D., Batchvarov, I., Nadeau, J.H., Capel, B., 2009. BAX-mediated cell death affects early germ cell loss and incidence of testicular teratomas in Dnd1(Ter/Ter) mice. Developmental biology 328, 377-383.

Cook, M.S., Munger, S.C., Nadeau, J.H., Capel, B., 2011. Regulation of male germ cell cycle arrest and differentiation by DND1 is modulated by genetic background. Development 138, 23-32.

Criscione, S.W., Zhang, Y., Thompson, W., Sedivy, J.M., Neretti, N., 2014. Transcriptional landscape of repetitive elements in normal and cancer human cells. BMC genomics 15, 583.

Dawson, E.P., Lanza, D.G., Webster, N.J., Benton, S.M., Suetake, I., Heaney, J.D., 2018. Delayed male germ cell sex-specification permits transition into embryonal carcinoma cells with features of primed pluripotency. Development 145.

Fuerer, C., Nostro, M.C., Constam, D.B., 2014. Nodal.Gdf1 heterodimers with bound prodomains enable serum-independent nodal signaling and endoderm differentiation. The Journal of biological chemistry 289, 17854-17871.

Greco, C.M., Kunderfranco, P., Rubino, M., Larcher, V., Carullo, P., Anselmo, A., Kurz, K., Carell, T., Angius, A., Latronico, M.V., Papait, R., Condorelli, G., 2016. DNA hydroxymethylation controls cardiomyocyte gene expression in development and hypertrophy. Nature communications 7, 12418.

Gross-Thebing, T., Yigit, S., Pfeiffer, J., Reichman-Fried, M., Bandemer, J., Ruckert, C., Rathmer, C., Goudarzi, M., Stehling, M., Tarbashevich, K., Seggewiss, J., Raz, E., 2017. The Vertebrate Protein Dead End Maintains Primordial Germ Cell Fate by Inhibiting Somatic Differentiation. Developmental cell 43, 704-715 e705.

Gu, W., Mochizuki, K., Otsuka, K., Hamada, R., Takehara, A., Matsui, Y., 2018. Dnd1-mediated epigenetic control of teratoma formation in mouse. Biology open 7.

Heaney, J.D., Anderson, E.L., Michelson, M.V., Zechel, J.L., Conrad, P.A., Page, D.C., Nadeau, J.H., 2012. Germ cell pluripotency, premature differentiation and susceptibility to testicular teratomas in mice. Development 139, 1577-1586.

Jameson, S.A., Natarajan, A., Cool, J., DeFalco, T., Maatouk, D.M., Mork, L., Munger, S.C., Capel, B., 2012. Temporal transcriptional profiling of somatic and germ cells reveals biased lineage priming of sexual fate in the fetal mouse gonad. PLoS genetics 8, e1002575.

Kanehisa, M., Furumichi, M., Tanabe, M., Sato, Y., Morishima, K., 2017. KEGG: new perspectives on genomes, pathways, diseases and drugs. Nucleic acids research 45, D353-D361.

Kedde, M., Strasser, M.J., Boldajipour, B., Vrielink, J.A., Slanchev, K., le Sage, C., Nagel, R., Voorhoeve, P.M., van Duijse, J., Orom, U.A., Lund, A.H., Perrakis, A., Raz, E., Agami, R., 2007. RNA-binding protein Dnd1 inhibits microRNA access to target mRNA. Cell 131, 1273-1286.

Kivioja, T., Vaharautio, A., Karlsson, K., Bonke, M., Enge, M., Linnarsson, S., Taipale, J., 2011. Counting absolute numbers of molecules using unique molecular identifiers. Nat Methods 9, 72-74.

Langmead, B., Trapnell, C., Pop, M., Salzberg, S.L., 2009. Ultrafast and memory-efficient alignment of short DNA sequences to the human genome. Genome biology 10, R25.

Lee, J.Y., Ji, Z., Tian, B., 2008. Phylogenetic analysis of mRNA polyadenylation sites reveals a role of transposable elements in evolution of the 3'-end of genes. Nucleic acids research 36, 5581-5590.

Lesch, B.J., Page, D.C., 2014. Poised chromatin in the mammalian germ line. Development 141, 3619-3626.

Madan, B., Madan, V., Weber, O., Tropel, P., Blum, C., Kieffer, E., Viville, S., Fehling, H.J., 2009. The pluripotency-associated gene Dppa4 is dispensable for embryonic stem cell identity and germ cell development but essential for embryogenesis. Mol Cell Biol 29, 3186-3203.

Matsui, Y., Zsebo, K., Hogan, B.L., 1992. Derivation of pluripotential embryonic stem cells from murine primordial germ cells in culture. Cell 70, 841-847.

McLaren, A., 1995. Germ cells and germ cell sex. Philosophical Transactions of the Royal Society of London 350, 229-233.

Nicholson, C.O., Friedersdorf, M.B., Bisogno, L.S., Keene, J.D., 2017. DO-RIP-seq to quantify RNA binding sites transcriptome-wide. Methods 118-119, 16-23.

Noguchi, T., Noguchi, M., 1985. A recessive mutation (ter) causing germ cell deficiency and a high incidence of congenital testicular teratomas in 129/Sv-ter mice. J Natl Cancer Inst 75, 385-392.

Pesce, M., Scholer, H.R., 2000. Oct-4: control of totipotency and germline determination. Molecular reproduction and development 55, 452-457.

Picelli, S., Faridani, O.R., Bjorklund, A.K., Winberg, G., Sagasser, S., Sandberg, R., 2014. Full-length RNA-seq from single cells using Smart-seq2. Nature Protocols 9, 171-181.

Ray, D., Kazan, H., Cook, K.B., Weirauch, M.T., Najafabadi, H.S., Li, X., Gueroussov, S., Albu, M., Zheng, H., Yang, A., Na, H., Irimia, M., Matzat, L.H., Dale, R.K., Smith, S.A., Yarosh, C.A., Kelly, S.M., Nabet, B., Mecenas, D., Li, W., Laishram, R.S., Qiao, M., Lipshitz, H.D., Piano, F., Corbett, A.H., Carstens, R.P., Frey, B.J., Anderson, R.A., Lynch, K.W., Penalva, L.O., Lei, E.P., Fraser, A.G., Blencowe, B.J., Morris, Q.D., Hughes, T.R., 2013. A compendium of RNA-binding motifs for decoding gene regulation. Nature 499, 172-177.

Robinson, M.D., McCarthy, D.J., Smyth, G.K., 2010. edgeR: a Bioconductor package for differential expression analysis of digital gene expression data. Bioinformatics 26, 139-140.

Saba, R., Kato, Y., Saga, Y., 2014. NANOS2 promotes male germ cell development independent of meiosis suppression. Developmental biology 385, 32-40.

Shimobayashi, M., Hall, M.N., 2014. Making new contacts: the mTOR network in metabolism and signalling crosstalk. Nature reviews. Molecular cell biology 15, 155-162.

Slagle, C.E., Aoki, T., Burdine, R.D., 2011. Nodal-dependent mesendoderm specification requires the combinatorial activities of FoxH1 and Eomesodermin. PLoS genetics 7, e1002072.
Spiller, C., Burnet, G., Bowles, J., 2017. Regulation of fetal male germ cell development by members of the TGFbeta superfamily. Stem Cell Res 24, 174-180.
Stevens, L.C., 1966. Development of resistance to teratocarcinogenesis by primordial germ cells in mice. J Natl Cancer Inst 37, 859-867.
Stevens, L.C., 1973. A new inbred subline of mice (129-terSv) with a high incidence of spontaneous congenital testicular teratomas. J Natl Cancer Inst 50, 235-242.
Stevens, L.C., Little, C.C., 1954. Spontaneous Testicular Teratomas in an Inbred Strain of Mice. Proceedings of the National Academy of Sciences of the United States of America 40, 1080-1087.
Suzuki, A., Niimi, Y., Saga, Y., 2014. Interaction of NANOS2 and NANOS3 with different components of the CNOT complex may contribute to the functional differences in mouse male germ cells. Biology open 3, 1207-1216.
Suzuki, A., Niimi, Y., Shinmyozu, K., Zhou, Z., Kiso, M., Saga, Y., 2016. Dead end1 is an essential partner of NANOS2 for selective binding of target RNAs in male germ cell development. EMBO reports 17, 37-46.
Suzuki, A., Saga, Y., 2008. Nanos2 suppresses meiosis and promotes male germ cell differentiation. Genes & development 22, 430-435.
Tanaka, C., Sakuma, R., Nakamura, T., Hamada, H., Saijoh, Y., 2007. Long-range action of Nodal requires interaction with GDF1. Genes & development 21, 3272-3282.
Updike, D.L., Knutson, A.K., Egelhofer, T.A., Campbell, A.C., Strome, S., 2014. Germ-granule components prevent somatic development in the C. elegans germline. Current biology : CB 24, 970-975.
Weidinger, G., Stebler, J., Slanchev, K., Dumstrei, K., Wise, C., Lovell-Badge, R., Thisse, C., Thisse, B., Raz, E., 2003. dead end, a novel vertebrate germ plasm component, is required for zebrafish primordial germ cell migration and survival. Current biology : CB 13, 1429-1434.
Western, P.S., Ralli, R.A., Wakeling, S.I., Lo, C., van den Bergen, J.A., Miles, D.C., Sinclair, A.H., 2011. Mitotic arrest in teratoma susceptible fetal male germ cells. PloS one 6, e20736.
Western, P.S., van den Bergen, J.A., Miles, D.C., Sinclair, A.H., 2010. Male fetal germ cell differentiation involves complex repression of the regulatory network controlling pluripotency. FASEB J 24, 3026-3035.
Yamaguchi, S., Kimura, H., Tada, M., Nakatsuji, N., Tada, T., 2005. Nanog expression in mouse germ cell development. Gene Expr Patterns 5, 639-646.
Yamaji, M., Jishage, M., Meyer, C., Suryawanshi, H., Der, E., Yamaji, M., Garzia, A., Morozov, P., Manickavel, S., McFarland, H.L., Roeder, R.G., Hafner, M., Tuschl, T., 2017. DND1 maintains germline stem cells via recruitment of the CCR4-NOT complex to target mRNAs. Nature 543, 568-572.
Yeom, Y.I., Fuhrmann, G., Ovitt, C.E., Brehm, A., Ohbo, K., Gross, M., Hubner, K., Scholer, H.R., 1996. Germline regulatory element of Oct-4 specific for the totipotent cycle of embryonal cells. Development 122, 881-894.
Yoshimizu, T., Sugiyama, N., De Felice, M., Yeom, Y.I., Ohbo, K., Masuko, K., Obinata, M., Abe, K., Scholer, H.R., Matsui, Y., 1999. Germline-specific expression of the Oct-

4/green fluorescent protein (GFP) transgene in mice. Dev Growth Differ 41, 675-684.
Youngren, K.K., Coveney, D., Peng, X., Bhattacharya, C., Schmidt, L.S., Nickerson, M.L., Lamb, B.T., Deng, J.M., Behringer, R.R., Capel, B., Rubin, E.M., Nadeau, J.H., Matin, A., 2005. The Ter mutation in the dead end gene causes germ cell loss and testicular germ cell tumours. Nature 435, 360-364.
Yu, F.X., Guan, K.L., 2013. The Hippo pathway: regulators and regulations. Genes & development 27, 355-371.
Zechel, J.L., Doerner, S.K., Lager, A., Tesar, P.J., Heaney, J.D., Nadeau, J.H., 2013. Contrasting effects of Deadend1 (Dnd1) gain and loss of function mutations on allelic inheritance, testicular cancer, and intestinal polyposis. BMC Genet 14, 54.
Zhu, R., Iacovino, M., Mahen, E., Kyba, M., Matin, A., 2011. Transcripts that associate with the RNA binding protein, DEAD-END (DND1), in embryonic stem (ES) cells. BMC Mol Biol 12, 37.